Development of the global maize production model MATCRO-Maize version 1.0

Marin Nagata[1], Astrid Yusara[2], Tomomichi Kato[3*], Yuji Masutomi[4]

[1]Graduate School of Global Food Resources, Hokkaido University, Sapporo, Hokkaido 060-0809, Japan
5 [2]Graduate School of Agriculture, Hokkaido University, Sapporo, Hokkaido 060-0808, Japan
[3]Research Faculty of Agriculture, Hokkaido University, Sapporo, Hokkaido 060-8589, Japan
[4]Center for Climate Change Adaptation, National Institute for Environmental Studies, Tsukuba, Ibaraki 305-8506, Japan

Correspondence to: Tomomichi Kato (tkato@agr.hokudai.ac.jp)

10 **Abstract.** Process-based crop models combined with land surface models are useful tools for accurately quantifying the impacts of climate change on crops while considering the interactions between agricultural land and climate. We developed a new process-based crop model for maize, named MATCRO-Maize, by incorporating leaf-level photosynthesis of C4 plants and adjusting crop-specific parameters into the original MATCRO model, which is a process-based crop model initially developed for paddy rice combined with a land surface model. The model was validated at both a point scale and a global

15 scale through comparisons with observational values. The validation at the point scale was conducted at four globally distributed sites. It showed statistically significant correlation for three variables (leaf area index: correlation coefficient (COR) of 0.76 with a p value < 0.01; total aboveground biomass: COR of 0.89 with a p value < 0.001; final yield: COR of 0.34 with a p value < 0.01). For the global scale validation, the simulated yield was statistically compared with the FAOSTAT data at the country level and total global level. Although the absolute value of the simulated yield tended to be

20 overestimated, MATCRO-Maize could capture spatial variability, as indicated by a COR of 0.58 (p value < 0.01) for the 30-year average yield comparison of the top 20 maize-producing countries. In addition, the comparisons of the interannual variability derived from detrended deviation were statistically significant for the total global yield (COR of 0.54 with p value < 0.01) and for half of the top 20 countries (COR of 0.64-0.90 with p value < 0.001 for 6 countries; COR of 0.50-0.51 with p value < 0.01 for 2 countries; COR of 0.48-0.55 with p value < 0.05 for 2 countries), which are comparable with those of

25 other global crop models. One of the reasons for this overestimation could be related to the strong nitrogen fertilization effect observed in MATCRO-Maize. With experimental field data under more comprehensive conditions, improvements in the functions of nitrogen fertilizer in the model would be needed to simulate the maize yield more accurately.

1 Introduction

30 Maize (*Zea mays* L.) is one of the most important cereals not only because of its large production (FAO, 2022) but also because of its various roles in human food, feed, and industrial uses. Maize has high photosynthetic efficiency as a C4 plant. It contains phosphoenolpyruvate (PEP) carboxylase in mesophyll cells, which concentrates CO_2 in bundle sheath cells. The concentrated CO_2 increases the relative amount of carboxylation versus oxygenation performed by ribulose-1,5-bisphosphate carboxylase/oxygenase (Rubisco) (Kanai and Edwards, 1999), allowing C4 plants to operate at lower stomatal conductance

35 rates than C3 plants (Sage, 1999). This mechanism results in high efficiencies of light, water, and nitrogen use (Knapp and Medina, 1999; Long, 1999). These features, such as multipurpose crops and high photosynthetic efficiency, enable the cultivated area to range over wide environments from wet to dry and from low to midlatitude. However, climate change impacts and climate-related extremes negatively affect the productivity of the agricultural sector, which leads to negative consequences for food security (Intergovernmental Panel on Climate Change (IPCC), 2023). Therefore, it is important to

40 accurately quantify the impact of climate change on crop growth and yield and to identify effective adaptation strategies to mitigate climate risk.

Process-based crop models are useful tools for climate change studies because they consider the response of the physiological processes of crop growth and development to the environment and management (Tubiello and Ewert, 2002). The ensemble of process-based crop model simulations has shown good agreement with observed maize yields both at the

45 site scale and at the global scale (Bassu et al., 2014; Jägermeyr et al., 2021), showing its potential to quantify the uncertainty in studies on the impacts of climate change on crop yields (Asseng et al., 2013). Crop models combined with land surface models (LSMs) or earth system models (ESMs) (as classified by Peng et al., 2017) have the ability to consider the effects of agricultural land on the climate globally through the exchange of fluxes of heat, water, and gases, as well as the effects of climate on crops. Some studies have revealed that agricultural land affects the climate through fluxes (Bondeau et al., 2007;

50 Levis et al., 2012; Maruyama and Kuwagata, 2010; Tsvetsinskaya et al., 2001) and subsequently affects crop production (Osborne et al., 2009). This indicates the importance of considering the interaction between agricultural land and climate to accurately quantify the impacts of climate change on crops. Despite this importance, few LSM/ESM-based crop models exist (Lin et al., 2021; Lombardozzi et al., 2020; Osborne et al., 2015; Wu et al., 2016).

MATCRO is a process-based crop growth model developed for C3 plants (Masutomi et al., 2016a, b; Yusara et al., in

55 prep). It was initially combined with a land surface model of Minimal Advanced Treatments of Surface Interaction and Runoff, called MATSIRO (Takata et al., 2003). MATSIRO is embedded in an earth system model, which is the Model for Interdisciplinary Research on Climate, Earth System version 2 for Long-term simulations called MIROC-ES2L (Hajima et al., 2020). MATCRO simulates crop growth based on leaf-level photosynthesis and parameterized crop-specific parameters determined from experimental data, and can run simulations both at a point scale and at a global scale. The model was

60 applied to assess the impact of climate change at the country and local levels (Kinose et al., 2020; Kinose and Masutomi, 2019) and was used in the study investigating factors to improve the simulation performance of global gridded crop models

(GGCMs) (Iizumi et al., 2021). MATCRO is applicable to other crops, including maize as a C4 plant, with adjusted parameters from experimental datasets and the literature.

We extended MATCRO for global maize yield simulation, called MATCRO-Maize, by adjusting crop-specific parameters for maize and incorporating the C4 photosynthetic mechanism. MATCRO-Rice can simulate latent heat flux, sensible heat flux, net carbon uptake by crops, and rice yield, indicating its application in studies on climate change impacts as an LSM-based model (Masutomi et al. 2016b). However, this study focused only on crop growth and yields, omitting water and heat fluxes to increase computational efficiency. This paper aims to describe MATCRO-Maize in detail (Section 2) and model validation on simulated yields both at a point scale and at a global scale (Section 3), with a discussion of the validation and model limitations (Section 4).

2. Model description

MATCRO consists of four modules: radiation, net carbon assimilation, crop growth, and soil water balance. It requires the following input data: (i) phenological data (i.e., crop calendar), (ii) water management data (i.e., the land is rainfed or irrigated), (iii) nitrogen fertilizer application data (N_{fert}) [kg N ha^{-1}], (iv) soil classification data (i.e., soil texture classification), (v) annual CO_2 data [ppm], and (vi) 6 types of daily meteorological data: air pressure (P_s) [Pa], precipitation (P_{rc}) [kg m^{-2} s^{-1}], specific humidity [S_h] [kg kg^{-1}], downwards shortwave radiation (R_s) [W m^{-2}], maximum, minimum, and mean air temperature (T_{max}, T_{min}, T_a) [K], and wind speed (U) [m s^{-1}]. Based on input data, MATCRO simulates crop growth during a growing period. It is controlled by the crop developmental stage (D_{vs}) based on (Bouman et al., 2001), which is the index used to quantify crop development. The final crop yield is determined by the dry weight of the storage organ with a parameter (K_{yld}) when $D_{vs} = 1$. To adapt MATCRO for maize, crop-specific parameters and equations were improved, as shown in Table 1 and Eq. (1)–(35). The details are described in the following sections.

2.1 Photosynthetic mechanism

MATCRO calculates net carbon assimilation for the entire canopy (A_n) via the big-leaf model (Dai et al., 2004), where C3 leaf-level photosynthesis is separately calculated for sunlit and shaded leaves from the coupled photosynthesis–stomatal conductance model (Collatz et al., 1991).

A_n for the entire canopy is given by:

$$A_n = \overline{A}_{n,sn} L_{sn} + \overline{A}_{n,sh} L_{sh}, \tag{1}$$

where $\overline{A}_{n,sn}$ and $\overline{A}_{n,sh}$ represent the net carbon assimilation per unit leaf area [μ mol m^{-2} s^{-1}] and where L_{sn} and L_{sh} represent the leaf area index (LAI) [m^2 (leaf) m^{-2}]. sn and sh indicate sunlit and shaded leaves, respectively. $\overline{A}_{n,sn}$ and $\overline{A}_{n,sh}$ are defined in the following equations:

$$\overline{A}_{n,x} = \overline{A}_{g,x} - \overline{R}_{d,x}, \tag{2}$$

where $\overline{A}_{g,x}$ and $\overline{R}_{d,x}$ represent gross carbon assimilation and dark respiration per unit leaf area [μ mol m^{-2} s^{-1}], respectively. Suffix x means sn or sh. L_{sn} and L_{sh} are determined following the approach of Masutomi et al., (2016a). $\overline{R}_{d,x}$ is calculated

95   via the following equation (Bonan et al., 2011):

$$\overline{R}_{d,x} = 0.025\, V_{cmax,x} \left(\frac{2^{(Tv-298.15)/10}}{1+\exp{(1.3(Tv-328.15))}} \right), \tag{3}$$

where $V_{cmax,x}$ [μ mol m^{-2} s^{-1}] is the maximum rate of carboxylation and where T_v is the leaf temperature [K] (assumed to be the same as the air temperature: T_a). $\overline{A}_{g,x}$ is determined by the smaller root of the following equations:

$$\beta_{cj}\overline{A}_{i,x}^2 - (\overline{A}_{c,x} + \overline{A}_{j,x})\overline{A}_{i,x} + \overline{A}_{c,x}\overline{A}_{j,x} = 0, \tag{4}$$

100   $$\beta_{ip}\overline{A}_{g,x}^2 - (\overline{A}_{i,x} + \overline{A}_{p,x})\overline{A}_{g,x} + \overline{A}_{i,x}\overline{A}_{p,x} = 0, \tag{5}$$

where β_{cj} and β_{ip} are the transition factors (Table 1) and where $\overline{A}_{i,x}$ [μ mol m^{-2} s^{-1}] is the colimited photosynthesis. Here, we introduced the C4 leaf-level photosynthesis model based on Collatz et al., (1992) into MATCRO, in which some parameters were taken from Oleson et al., (2013) and Lawrence et al., (2020) (Table 1). In C4 photosynthesis, $\overline{A}_{c,x}$, $\overline{A}_{j,x}$, and $\overline{A}_{p,x}$ [μ mol m^{-2} s^{-1}] represent Rubisco-limited, RUBP-limited, and PEP-limited photosynthesis, respectively, and are given by the

105   following equations:

$$\overline{A}_{c,x} = V_{cmax,x}, \tag{6}$$

$$\overline{A}_{j,x} = \alpha(4.6Q_{ab,x}), \tag{7}$$

$$\overline{A}_{p,x} = k_{p,x}C_{i,x}, \tag{8}$$

where $C_{i,x}$ [ppm] is the internal leaf CO_2 concentration, $Q_{ab,x}$ [W m^{-2}] is the absorbed photosynthetically active radiation

110   (PAR), α [mol mol^{-1}] is the quantum efficiency, and $k_{p,x}$ [μ mol m^{-2} s^{-1}] is the initial slope of the CO_2 response curve for the C4 CO_2 response curve. $Q_{ab,x}$ is calculated from R_s via the same methods as in Masutomi et al. (2016a) and is converted to photosynthetic photon flux by multiplying by 4.6 [μ mol (photons) J^{-1}]. $V_{cmax,x}$ and $k_{p,x}$ are functions of T_v and are based on Lawrence et al. (2020),

$$V_{cmax,x} = f_v\, V_{cmax25,x} \left[\frac{Q_{10}^{(T_v-298.15)/10}}{f_H(T_v)f_L(T_v)} \right], \tag{9}$$

115   $$f_H(T_v) = 1 + exp[S_1(T_v - S_2)], \tag{10}$$

$$f_L(T_v) = 1 + exp[S_3(S_4 - T_v)], \tag{11}$$

$$k_{p,x} = \begin{cases} k_{p25,x}Q_{10}^{(T_v-298.15)/10}, & V_{cmax25,x} > 0, \\ 0.7\mu, & V_{cmax25,x} = 0, \end{cases} \tag{12}$$

$$k_{p25,x} = 20000V_{cmax25,x}, \tag{13}$$

with $Q_{10} = 2$, $S_1 = 0.3\,K^{-1}$, $S_2 = 313.15K$, $S_3 = 0.2\,K^{-1}$, and $S_4 = 288.15K$ (Table 1). Notably, $k_{p,x}$ is adjusted to be

120   0.7μ (Collatz et al., 1992) when $V_{cmax25,x} = 0$ because of the process of the photosynthesis calculation (Eq. (20)). $V_{cmax25,x}$

is the maximum Rubisco carboxylation rate per unit leaf area at 25℃ (the details are described in Section 2.2.2). f_v is the water stress factor calculated in the soil water balance module, which indirectly affects A_n through $V_{cmax,x}$ (Sellers et al., 1996). f_v is derived from the following equations:

$$f_v = \sum_{i=1}^{NSL} \begin{cases} 1 * ETF(i), & FAW(i) > 0.45, \\ \frac{FAW(i)}{0.45} * ETF(i), & otherwise, \end{cases} \tag{14}$$

$$FAW(i) = \min\left(\frac{\max\left((WSL(i)-WILT),0\right)}{FC-WILT}, 1\right), \tag{15}$$

$$ETF(i) = \frac{3}{2} \frac{(z_{rt}^2 - z^2)}{z_{rt}^3}, \tag{16}$$

where NSL represents the number of soil layers, ETF represents the fraction of transpiration from root distribution, FAW represents the fraction of available water, WSL represents the soil water content [m³ m⁻³], $WILT$ represents the wilting point, FC represents the field capacity, and z_{rt} and z represent the root depth and the soil depth, respectively, for each layer.

MATCRO assumes $NSL = 5$, where each of the soil layers has thicknesses of 0.05, 0.2, 0.75, 1, and 2 [m], respectively. MATCRO uses the soil texture data as input data, where the soil is classified into 13 types, leading to differences in $WILT$ and FC based on Campbell and Norman (1998). WSL is calculated considering transpiration from the canopy, evaporation from the soil, and water flux (those calculations are the same as those of the original MATCRO). The ETF calculation assumes that the root has no spatial orientation and is equally distributed in the soil (Masutomi et al., 2016a). z_{rt} is determined by the same calculation as the original MATCRO, where the crop-specific parameter ($z_{rt,mx}$) was changed to maize (Table 1). The conditional branch ($FAW(i) > 0.45$) is based on the FAO 56 guidelines (Allen et al., 1998).

Stomatal conductance influences CO_2 uptake during photosynthesis. MATCRO-Maize represents stomatal conductance for CO_2, $G_{sc,x}$ [μ mol m⁻² s⁻¹], based on Ball et al. (1987) as follows:

$$G_{sc,x} = \begin{cases} G_{0c} + G_{1c} R_h \frac{\overline{A_{n,x}}}{C_{s,x}}, & \overline{A}_{n,x} \geq 0, \\ G_{0c}, & otherwise, \end{cases} \tag{17}$$

where $C_{s,x}$ [ppm] is the CO_2 concentration at the leaf surface and where R_h [-] is the relative humidity at the leaf surface. G_{0c} and G_{1c} are derived from parameters b and m (shown in Table 1), respectively, by adjusting their ratio of 1:1.6, which is the ratio of diffusivity of H_2O to CO_2. Here, the leaf-level net carbon assimilation rate ($\overline{A}_{n,x}$), stomatal conductance for CO_2 ($G_{sc,x}$), and boundary layer conductance for CO_2 (G_{bc}) meet the following physical flux equations:

$$\overline{A}_{n,x} = G_{sc,x}\left(C_{s,x} - C_{i,x}\right), \tag{18}$$

$$\overline{A}_{n,x} = G_{bc}\left(C_a - C_{s,x}\right), \tag{19}$$

where C_a [ppm] is the atmospheric CO_2 concentration. G_{bc} is a function of air pressure (P_s [Pa]) and the wind speed in the canopy (U [m s⁻¹]) (Masutomi, 2023).

Here, T_v, $Q_{ab,x}$, R_h, U, and C_a are environmental variables derived from input meteorological climate data. There are four relationships (Eqs. (2), (17)-(19)) in terms of internal variables ($\overline{A}_{n,x}$, $G_{sc,x}$, $C_{s,x}$, $C_{i,x}$). MATCRO for C3 photosynthesis

obtains analytical solutions from relationships via the method shown in Masutomi (2023). For C4 photosynthesis, it is also possible to solve these equations analytically. In the case of Rubisco-limited and RuBP-limited photosynthesis, exact expressions for $\overline{A}_{c,x}$ and $\overline{A}_{j,x}$ are obtained. Under $\overline{A}_{n,x} \geq 0$, PEP-limited photosynthesis ($\overline{A}_{p,x}$) can be represented by quadratic equations by the algebraic procedures as follows:

$$0 = \left\{G_{bc}^2 G_{1c} R_h - G_{bc} G_{0c} - k_{p,x}(G_{0c} - G_{bc} G_{1c} R_h + G_{bc})\right\} \overline{A}_{p,x}^{\,2} + \left\{C_a G_{bc}^2 G_{0c} - G_{bc} G_{0c} R_d + G_{bc}^2 G_{1c} R_h R_d - \right.$$

$$\left. k_{p,x} C_a (G_{bc}^2 G_{1c} R_h - 2G_{bc} G_{0c} - G_{bc}^2)\right\} \overline{A}_{p,x} + C_a G_{bc}^2 G_{0c}(R_d - k_{p,x} C_a). \tag{20}$$

Under $\overline{A}_{n,x} < 0$, the PEP-limited photosynthesis rate can be expressed as

$$\overline{A}_{p,x} = \frac{k_{p,x} C_a - R_d}{1 + k_{p,x}\left(\frac{1}{G_{bc}} + \frac{1}{G_{0c}}\right)}. \tag{21}$$

According to these equations, in the case of PEP-limited photosynthesis, there are three possible solutions. Following the criteria described by Masutomi (2023), only one analytical solution can be selected when the following requirements are satisfied: (i) under $\overline{A}_{n,x} \geq 0$, the solution must be a positive or zero real solution, and under $\overline{A}_{n,x} < 0$, it must be a negative real solution; (ii) $G_{sc,x} > 0$; and (iii) $C_i > 0$.

2.2 Crop-specific parameterization

2.2.1 Phenology

The crop growing period in MATCRO is controlled by D_{vs} based on Bouman et al. (2001). Here, $D_{vs} = 0$ means sowing, and $D_{vs} = 1$ means maturity (harvesting). It is calculated from the following equations:

$$D_{vs} = G_{dd}/G_{dd,m}, \tag{22}$$

$$G_{dd} = \int_0^t D_{vr}\, dt', \tag{23}$$

$$D_{vr} = \begin{cases} 0, & T_t < T_b \mid T_h \leq T_t, \\ T_t - T_b, & T_b \leq T_t < T_o, \\ \frac{(T_b - T_o)(T_t - T_h)}{(T_h - T_o)}, & T_o \leq T_t < T_h, \end{cases} \tag{24}$$

where G_{dd} is the growing degree days at t (time), $G_{dd,m}$ is the growing degree day at maturity, D_{vr} is the developmental rate at time t, and T_t is the temperature at time t. T_b, T_h, and T_o are the crop-specific cardinal temperatures (minimum, maximum, and optimal temperatures for development, respectively, as shown in Table 1). $G_{dd,m}$ were parameterized for each point scale simulation and global scale simulation (Section 2.3). In addition, one parameter that represents the timing of flowering ($D_{vs,flw}$) was parameterized based on observational data for the point scale simulation (Table 1).

2.2.2 Leaf nitrogen and Rubisco capacity

Maximum Rubisco carboxylation rate

$V_{cmax25,x}$ used in the photosynthesis module (Section 2.1) is obtained by dividing the maximum Rubisco carboxylation rate at the canopy level ($V_{cmax25,x}(l)$) by L_x separately for sunlit and shaded leaves based on Bonan et al. (2011). The vertical distribution of $V_{cmax25}(l)$, which is the sum of $V_{cmax25,sn}(l)$ and $V_{cmax25,sh}(l)$, follows the exponential profile:

$$V_{cmax25}(l) = V_{cmax25}(0) \exp(-K_n l), \tag{25}$$

180 where $V_{cmax25}(0)$ is the maximum Rubisco carboxylation rate at the canopy top, K_n is a parameter for the vertical distribution of nitrogen (Table 1), and l represents the LAI depth from the top. The maximum Rubisco carboxylation rate in sunlit leaves ($V_{cmax25,sn}(l)$) is also calculated by the same relationship considering the light distribution:

$$V_{cmax25,sn}(l) = V_{cmax25}(0)[1 - exp(-l(K_n + K))]\frac{1}{K_n+K}, \tag{26}$$

where K is the direct beam extinction coefficient (the calculation is the same as that for Masutomi et al., 2016a).
185 $V_{cmax25,sh}(l)$ is given by the subtraction of Eq. (25) and Eq. (26).

Here, while Bonan et al. (2011) uses the fixed $V_{cmax25}(0)$ value in each plant functional type, $V_{cmax25}(0)$ in MATCRO is calculated dynamically as a function of specific leaf nitrogen (S_{ln} [g N m^{-2}]). The function is established based on the experimental literature data. Notably, we applied the relationship between S_{ln} and light-saturated CO$_2$ assimilation (A_{max}) from the literature, although MATCRO-Rice and MATCRO-Soybean utilize the direct relationship between S_{ln} and
190 $V_{cmax25}(0)$ based on the experimental literature data. The reasons are that we assume that A_{max} could be used as Rubisco-limited photosynthesis in C4 photosynthesis and that Rubisco-limited photosynthesis could be equal to the maximum Rubisco carboxylation rate from Eq. (6). Several studies have shown that A_{max} has a close relationship with S_{ln}, as shown by the logistic equation for maize (Drouet and Bonhomme, 2004; Muchow and Sinclair, 1994; Paponov and Engels, 2003; Paponov et al., 2005; Sinclair and Horie, 1989; Vos et al., 2005). We used two functions from them for different D_{vs} as
195 follows:

$$V_{cmax25}(0) = \begin{cases} 45.1 * \left\{ \frac{2}{1+\exp[-2.9*(S_{ln}-0.25)]} - 1 \right\}, & D_{vs} < D_{vs,flw}, \\ 40.2 * \left\{ \frac{2}{1+\exp[-1.41*(S_{ln}-0.43)]} - 1 \right\}, & D_{vs} \geq D_{vs,flw}, \end{cases} \tag{27}$$

where $D_{vs} < D_{vs,flw}$ represents the vegetative stage at which the equation was based on Vos et al. (2005); then, for the reproductive stage, the equation was from Drouet and Bonhomme (2004).

200 **Specific leaf nitrogen**

S_{ln}, which is used in the calculation of $V_{cmax25}(0)$, is obtained from the function of D_{vs} in MATCRO. The function is established based on the observational data. We utilized the study by Muchow (1988), in which S_{ln} was measured under various levels of N_{fert} (0, 60, 120, 240, 420 [kg ha^{-1}]), as follows: (i) we traced S_{ln} data using digitizer software (https://apps.automeris.io/wpd4/) and obtained the measurement and phenological data from the paper; and (ii) we conducted
205 the fitting based on the assumption that S_{ln} linearly increased until flowering and then decreased towards maturity. The parameterization given by Eqs. (28)-(30) is shown in Figure 1.

$$
S_{ln} = \begin{cases} \frac{S_{ln,mx} - S_{ln,plt}}{D_{vs,flw}} D_{vs} + S_{ln,plt}, & D_{vs} < D_{vs,flw}, \\ \frac{S_{ln,matu} - S_{ln,mx}}{1 - D_{vs,flw}} (D_{vs} - 1) + S_{ln,matu}, & D_{vs} \geq D_{vs,flw}, \end{cases}
\tag{28}
$$

where $S_{ln,matu}$, $S_{ln,mx}$, and $S_{ln,plt}$ are S_{ln} at maturity, maximum S_{ln}, and S_{ln} at planting, respectively (Table 1). $S_{ln,mx}$ and $S_{ln,matu}$ are empirically parameterized as functions of N_{fert} as follows:

210

$$
S_{ln,mx} = \begin{cases} -0.00001\, N_{fert}^2 + 0.0064\, N_{fert} + 0.6891, & N_{fert} \leq 240, \\ 1.75, & N_{fert} > 240. \end{cases}
\tag{29}
$$

$$
S_{ln,matu} = \begin{cases} 0.001\, N_{fert} + 0.57, & N_{fert} \leq 240, \\ 1, & N_{fert} > 240. \end{cases}
\tag{30}
$$

We set fixed values of 1.75 for $S_{ln,mx}$ and 1.0 for $S_{ln,matu}$ when N_{fert} exceeds 240 [kg ha^{-1}], as $S_{ln,mx}$ and $S_{ln,matu}$ exhibit minimal increases beyond this threshold.
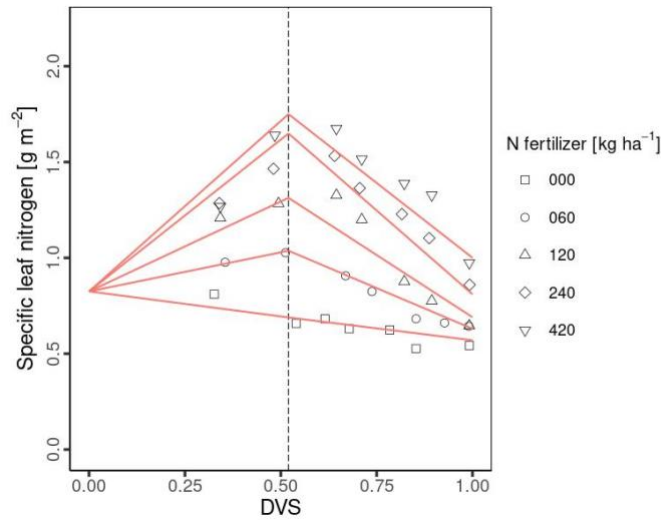
215 **Figure 1.** Relationship between developmental stage ($\boldsymbol{D_{vs}}$) and specific leaf nitrogen ($\boldsymbol{S_{ln}}$) in MATCRO-Maize. Shapes show observational data from Muchow (1988) with the 5 types of $\boldsymbol{N_{fert}}$: 0 kg ha^{-1} (square), 60 kg ha^{-1} (cycle), 120 kg ha^{-1} (triangle), 240 kg ha^{-1} (diamond), and 420 kg ha^{-1} (inverted triangle). The red lines represent the fitted line parameters used in MATCRO-Maize, while the dashed line represents $\boldsymbol{D_{vs}}$ at flowering ($\boldsymbol{D_{flw}}$).

2.2.3 Crop growth

220 **Glucose partitioning**

MATCRO calculates crop growth by partitioning net carbon assimilation (A_n) in the form of glucose, which is calculated in the photosynthesis module (Section 2.1). Partitioned glucose is supplied through photosynthesis in leaves and remobilization from the stem. The ratio of glucose partition to each organ (leaf, stem, root, and storage organ; ear) depends on D_{vs}. The term "ear" in maize represents the reproductive organ responsible for grain development. The dry matter for each organ is

225 obtained from the partitioned glucose considering the carbon fraction for each organ ($C_{glu,ear}$, $C_{glu,leaf}$, $C_{glu,rot}$, $C_{glu,stm}$ in

Table 1). We parameterized the partitioning ratio to leaf, stem, and ear based on the observational biomass data from Ciampitti et al. (2013a, b), whereas the ratio to shoots/roots was derived from the value from Penning de Vries et al. (1989). Figure 2 shows the partition ratio to the leaf ($P_{r,lef}$) and ear ($P_{r,ear}$) established via the following equations:

$$P_{r,lef} = \begin{cases} P_{lef}, & D_{vs} < D_{vs,lef1}, \\ \frac{P_{lef}(D_{vs,lef2} - D_{vs})}{D_{vs,lef2} - D_{vs,lef1}}, & D_{vs} < D_{vs,lef2}, \\ 0, & otherwise, \end{cases} \tag{31}$$

230

$$P_{r,ear} = \begin{cases} 0, & D_{vs} < D_{vs,ear1}, \\ \frac{D_{vs} - D_{vs,ear1}}{D_{vs,ear2} - D_{vs,ear1}}, & D_{vs} < D_{vs,lef2}, \\ 1, & otherwise, \end{cases} \tag{32}$$

where $D_{vs,lef1}$, $D_{vs,lef2}$, $D_{vs,ear1}$ and $D_{vs,ear2}$ represent the D_{vs} at which the corresponding partition changes, as determined in Table 1 based on Figure 2, and where P_{lef} is the ratio of glucose partitioned to glucose to the leaf from glucose partitioned to the shoot.
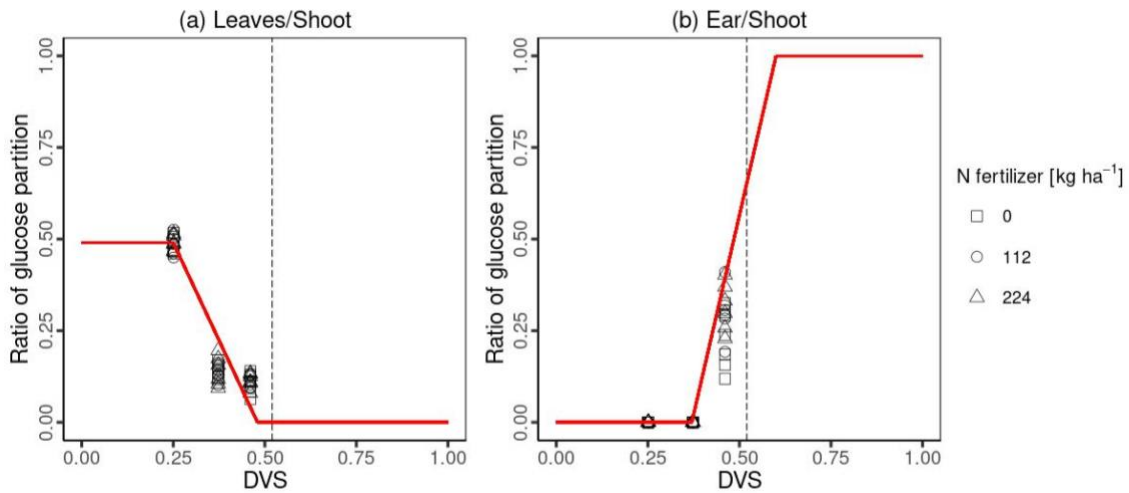

235 **Figure 2.** The ratio of glucose partitioning to leaves (a) and ears (b). Points show the ratio of glucose partition with different N_{fert}: 0 kg ha^{-1} (square), 112 kg ha^{-1} (cycle), and 224 kg ha^{-1} (triangle) measured in Ciampitti et al. (2013a, b). The red lines in Figure 2 show the fitted line parameters used in MATCRO-Maize, while the dashed line represents D_{vs} at flowering ($D_{vs,flw}$).

Specific leaf weight

240 The specific leaf weight (S_{lw}) is used to calculate the total leaf area index (L) in MATCRO. It is a function of D_{vs} and is given by:

$$S_{lw} = S_{lw,mx} + (S_{lw,mn} - S_{lw,mx})\exp(-k_{Slw}D_{vs}) \tag{33}$$

where $S_{lw,mn}$, $S_{lw,mx}$, and k_{Slw} are crop-specific parameters derived from the observational data expressed in Table 1. We conducted curve fitting to S_{lw} calculated from the dry weight of the leaf biomass and the leaf area index based on Ciampitti

245 et al. (2013a, b) and established a relationship (Figure 3).
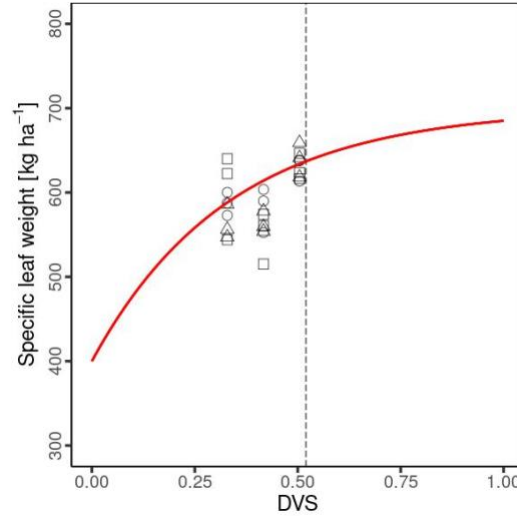
Figure 3. Relationships between specific leaf weights and developmental stages. Similar to Fig. 2.

2.2.4 Crop height

Crop height (H_{gt}) is related to the calculation of evaporation in MATCRO. It assumes that the dependence of the crop height

250 on D_{vs} is based on Penning de Vries et al. (1989) and is given by

$$H_{gt} = \begin{cases} h_{aa}D_{vs}/D_{vs,flw}, & D_{vs} < D_{vs,flw} \\ h_{aa}, & D_{vs} \geq D_{vs,flw} \end{cases} \tag{34}$$

where h_{aa} is the crop height at flowering, as shown in Table 1.

2.2.5 Crop yield

MATCRO calculates the final crop yield, Y_{ld}, from the dry weight of the storage organ at maturity ($W_{ear,mt}$) as follows:

255 $$Y_{ld} = k_{yld}W_{ear,mt}. \tag{35}$$

Here, k_{yld} is the crop-specific parameter (Table 1), which represents the ratio of Y_{ld} to $W_{ear,mt}$. We parameterized K_{yld}

based on Ciampitti et al. (2013b).

Table 1. Parameters in MATCRO-Maize

Variable	Value	Units	Description	Source
Crop-specific	(maize)			
b	0.04	mol (H_2O) m^{-2} s^{-1}	intercept of the Ball-Berry model	Sellers et al., (1996)
$C_{glu,ear}$	0.815	ratio	conversion factor of dry weight from glucose to ear	Penning de Vries et al., (1989)
$C_{glu,leaf}$	0.871	ratio	conversion factor of dry weight from glucose to leaf	Penning de Vries et al., (1989)
$C_{glu,rot}$	0.857	ratio	conversion factor of dry weight from glucose to root	Penning de Vries et al., (1989)
$C_{glu,stm}$	0.810	ratio	conversion factor of dry weight from glucose to stem	Penning de Vries et al., (1989)
$D_{vs,rot1}$	0.35	ratio	1st point of D_{vs} at which the partition pattern to root changes	Penning de Vries et al., (1989)

Variable	Value	Units	Description	Source
Crop-specific	**(maize)**			
$D_{vs,rot2}$	0.72	ratio	2nd point of D_{vs} at which the partition pattern to root changes	Penning de Vries et al., (1989)
$D_{vs,ear1}$	0.37	ratio	1st point of D_{vs} at which the partition pattern to ear changes	Parameterized in this study
$D_{vs,ear2}$	0.6	ratio	2nd point of D_{vs} at which the partition pattern to ear changes	Parameterized in this study
$D_{vs,flw}$	0.52	ratio	D_{vs} at flowering	Parameterized in this study
$D_{vs,lef1}$	0.25	ratio	1st point of D_{vs} at which the partition pattern to leaf changes	Parameterized in this study
$D_{vs,lef2}$	0.48	ratio	2nd point of D_{vs} at which the partition pattern to leaf changes	Parameterized in this study
f_{stc}	0.35	ratio	fraction of glucose allocated to starch reserves	Penning de Vries et al., (1989)
h_{aa}	2	m	crop height at flowering	Penning de Vries et al., (1989)
k_{yld}	0.83	ratio	ratio of crop yield to dry weight of ear at maturity	Parameterized in this study
k_{Slw}	3	ratio	parameter that represents the relationship between S_{lw} and D_{vs}	Parameterized in this study
m	4	ratio	the slope of the Ball-Berry model	Sellers et al., (1996)
$G_{dd,m}$	–	K day	growing degree day at maturity	Parameterized in this study
P_{lef}	0.49	ratio	partition ratio of glucose to leaf from glucose partitioned to the shoot	Parameterized in this study
P_{rot}	0.25	ratio	partition ratio of glucose to root	Penning de Vries et al., (1989)
$r_{dl,lef}$	3.0×10^{-7}	s^{-1}	ratio of dead leaf at harvest	Masutomi et al., (2016)
r_{rt}	0.06	m s^{-1}	growth ratio of root	Penning de Vries et al., (1989)
$S_{ln,plt}$	0.825	g m^{-2}	specific leaf nitrogen at planting	Parameterized in this study
$S_{ln,mx}$	See Eq. (29)	g m^{-2}	maximum specific leaf nitrogen	Parameterized in this study
$S_{ln,matu}$	See Eq. (30)	g m^{-2}	specific leaf nitrogen at maturity	Parameterized in this study
$S_{lw,mn}$	400	kg ha^{-1}	minimum specific leaf weight	Parameterized in this study
$S_{lw,mx}$	700	kg ha^{-1}	maximum specific leaf weight	Parameterized in this study
T_b	281.75	K	minimum temperature for development	Osborne et al., (2015)
T_h	315.15	K	maximum temperature for development	Osborne et al., (2015)
T_o	303.15	K	optimal temperature for development	Osborne et al., (2015)
$z_{rt,mx}$	1.5	m	maximum root depth	Penning de Vries et al., (1989)
α	0.05	mol mol^{-1}	quantum efficiency	Sellers et al., (1996)
β_{cj}	0.8	ratio	GPP transition factor	Lawrence et al., (2020)
Others				
k_n	0.3	ratio	vertical distribution of nitrogen	Oleson et al., (2013)
S_1	0.3	K^{-1}	temperature dependence of $V_{cmax,x}$	Lawrence et al., (2020)
S_2	313.15	K	temperature dependence of $V_{cmax,x}$	Lawrence et al., (2020)
S_3	0.2	K^{-1}	temperature dependence of $V_{cmax,x}$	Lawrence et al., (2020)
S_4	288.15	K	temperature dependence of $V_{cmax,x}$	Lawrence et al., (2020)
β_{ip}	0.95	ratio	GPP transition factor	Lawrence et al., (2020)

2.3 Model validation

260   MATCRO can run the simulation both at a point scale and at a global scale. The developed model was validated both at a point scale and at a global scale. For point scale validation, the three model output datasets, LAI, total aboveground biomass,

and yield, were compared with the observation data from the four sites. After confirming the ability of the model to simulate maize growth, two types of validations were conducted at the global scale. First, the simulated yields at the grid cell were compared with the gridded yield data of the Global Dataset of Historical Yields (GDHY) (Iizumi, 2019). Second, the simulated yields at the country and total global levels were compared with the country yield report and global data from the Food and Agriculture Organization (FAOSTAT, 2024). To quantify the model performance, four statistical values were used in this study: the Pearson correlation coefficient (COR), root mean square error (RMSE), relative root mean square error (RRMSE) and normalized mean absolute error (NMAE). RRMSE and NMAE were calculated as follows:

$$RMSE = \sqrt{\frac{1}{n}\sum_{i=1}^{n}(y_i - \hat{y}_i)^2},$$ (36)

$$RRMSE = \frac{RMSE}{\overline{Y}},$$ (37)

$$NMAE = \frac{1}{n}\sum_{i=1}^{n}\frac{|\hat{y}_i - y_i|}{y_i},$$ (38)

where y_i is the actual value, $\hat{y}_i$ is the predicted value, and $\overline{Y}$ is the mean of the actual value.

2.3.1 Model validation at a point scale

To validate the model accuracy at a field scale, we used observational data from four sites (Brazil, France, Tanzania, and the USA; Table 2) used in the Agricultural Model Intercomparison and Improvement Project (AgMIP) study (Bassu et al., 2014). We used local daily climate data of precipitation, downwards shortwave radiation, air temperature, wind speed (P_{rc}, R_s, T_a, U respectively), management data (N_{fert} and irrigation regime) and phenological data (planting, flowering, and maturity dates) for model input data at each site. There was no information on the classification of soil texture, so we extracted one grid dataset from the same data used for the global simulation (Section 2.3.2). Annual CO_2 data were also taken from the same data used for the global simulation. Climatic data were estimated from the NASA Modern Era Retrospective-Analysis for Research and Applications (MERRA; Rienecker et al., 2011) when measured data were unavailable (Bassu et al., 2014).

Table 2. Validation site information in the point-scale simulation

Country	Site	Latitude	Longitude	Soil type	Sowing date	Hybrid	Total N fertilizer [kg N ha⁻¹]	Irrigation
Brazil	Rio Verde	17.52°S	51.43°W	Geri-Gibbsic Ferralsol	Oct. 22nd 2003	Pioneer 30K75	0	No
France	Lusignan	46.25°N	00.07°E	Cambisol	Apr. 26th 1996	Furio	255	Yes
Tanzania	Morogoro	06.50°S	37.39°E	Haplic Arenosol	Oct. 26th 2009	TMV1	61	Yes
USA	Iowa	42.01°N	93.45°W	Gleysols	May 4th 2010	Golden Harvest GH-9014	167	No

Notably, air pressure (P_s) and specific humidity (S_h) were not provided. We used the same data as the global simulation for the soil classification and P_s. S_h was converted from R_h using T_a and the vapour pressure. We parameterized $G_{dd,m}$ and

$D_{vs,flw}$ based on T_a and phenological data (sowing, flowering, and maturity dates). $G_{dd,m}$ parameterized for each site is used

for the simulations, while the average $D_{vs,flw}$ over the 4 sites is used (0.52 in Table 1). As a result, the mean average errors

290   were estimated as 4.25 and 7 days for flowering and maturity, respectively (Figure 4). MATCRO was run with these

parameters, and then the model output was validated with the observations for the following 3 variables: seasonal change in

the LAI, total aboveground biomass, and final yield.
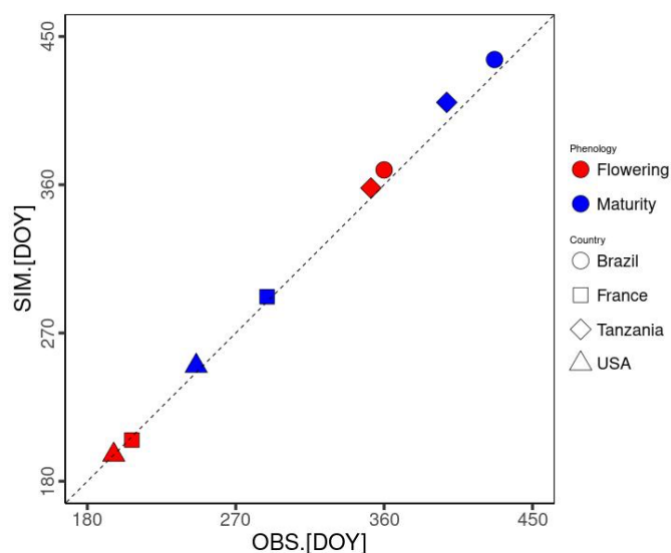
Figure 4. Comparison of the flowering and maturity date simulations (SIM on the y-axis) and observations (OBS on the x-axis). DOY represents the number of days from January 1st. Shapes show each site: Brazil (square), France (circle), Tanzania (triangle), and the USA (diamond). The colours indicate the phenological stages: flowering (red) and maturity (blue).

2.3.2 Model validation at a global scale

Simulation settings

300   For the global-scale simulation, the model was run at a spatial resolution of 0.5° × 0.5° from 1980–2010 under both rainfed

and irrigated conditions. The required input data were as follows. (i) Crop calendar data were from the Global Gridded Crop

Model Intercomparison (GGCMI) phase 3 protocol (Jägermeyr et al., 2021). It provides planting and maturity dates for 18

different crops, including maize, separated by rainfed and irrigated systems. We parameterized the average $G_{dd,m}$ at each

grid over the period 1980-2010 for the growing season from the planting to maturity dates for each of the rainfed and

305   irrigated conditions. Both the planting date and the simulated $G_{dd,m}$ were used as the input data for the global-scale

simulations. (ii) Water management data (i.e., irrigation regime) from the MIRCA2000 dataset (Portmann et al., 2010). In

the case of irrigated conditions, the soil moisture was set to field capacity during the growing season. (iii) N_{fert} from the

Inter-Sectoral Impact Model Intercomparison Project (ISIMIP; Volkholz and Ostberg, 2022). It provides the annual nitrogen

fertilizer inputs for five canonical crop types, including C4 annual crops for maize. (iv) Soil texture classification from

310   ISIMIP3a protocol soil input data (Volkholz and Müller, 2020). (v) Annual atmospheric CO_2 data from the ISIMIP3a (Büchner and Reyer, 2022). (vi) Six types of daily meteorological for model inputs (P_s, P_{rc}, S_h, T_{max}, T_{min}, T_a, U) from the GSWP3-W5E5 dataset for the ISIMIP3a dataset (Lange et al., 2022). We set the data from (i), (ii), and (iv) as constants across the simulation period, whereas the data from (iii), (v), and (vi) are variables.

315   **Analysis**

The simulated final yields in each grid cell under irrigated and rainfed conditions were aggregated by grid cell, country and global level with the harvested area from MIRCA2000 data (Portmann et al., 2010) via the following equation for each year from 1981-2010:

$$Yield_{aggregated} = \frac{\sum_{i=1}^{n}(Yield_{i,rf} \times Area_{i,rf}) + \sum_{i=1}^{n}(Yield_{i,irr} \times Area_{i,irr})}{\sum_{i=1}^{n}(Area_{i,rf} + Area_{i,irr})} \tag{39}$$

320   where $Yield_{aggregated}$ is the aggregated yield with the total grid cells (n) in grid cell i. $Yield_{rf}$ and $Yield_{irr}$ are the simulated yields under rainfed and irrigated conditions, respectively, and $Area_{rf}$ and $Area_{irr}$ are the harvested areas from MIRCA2000 for rainfed and irrigated conditions, respectively.

The model performance was evaluated by comparing its output with the historical yield dataset. The grid cell-level yield was averaged across a 30-year period and compared with the Global Dataset of Historical Yields (GDHY) (Iizumi, 2019).

325   The country- and global-level yields were compared with FAOSTAT data (FAOSTAT, 2024) for the average and annual variabilities over the 30 years. In the comparison at the country level, we focus on the top 20 maize-producing countries that account for more than 85% of total maize production.

We focused on two perspectives for validation: (i) the ability of the model to capture the spatial distribution of yield in both low- and high-producing countries and (ii) the ability of the model to reproduce the climatic effect reflected in the

330   interannual variability at the country and global scales. The first perspective was analysed using NMAE to quantify model error for both the global yield and the yield of the top 20 producing countries. The 30-year average yields were also compared on the basis of the statistics of COR, RMSE, and RRMSE to confirm the accuracy. The second perspective was analysed via the COR of the detrended deviation between the simulated and FAOSTAT yields to assess the interannual variability.

335

The effects of photosynthesis and N fertilizer

In addition to the yield comparison, we analysed the effect of nitrogen fertilizer (N_{fert}) on maize yield, as it is a key determinant of crop yield. This analysis compared both FAOSTAT data and simulated data from N_{fert} for a 30-year average with simple linear regression. We also conducted two tests to quantify the effects of the N_{fert}-related function and

340   parameters as follows: (i) Eq. (27) during the vegetative stage is derived from Drouet and Bonhomme (2004), defined as "test S_{ln}-V_{cmax}", was changed to:

$$V_{cmax}(0) = 36.8 * \left\{ \frac{2}{1+\exp[-2.45*(S_{ln}-0.27)]} - 1 \right\}, D_{vs} < D_{vs,flw} \tag{40}$$

and (ii) $S_{ln,plt}$ from 0.825 (Table 1) to 0.5 (defined as "test $S_{ln,plt}$").

## 3 Results

3.1 Point-scale simulations

A comparison of the time series changes in the LAI at each experimental site is shown in Figure 5. In general, MATCRO-Maize captured the increasing trend towards flowering time and then decreasing trend towards the end of maturity. Especially during the vegetative stage ($D_{vs} < D_{vs,flw}$: 0.52), the simulated LAI showed relatively good agreement. However, the simulated LAI was notably underestimated in Brazil and France immediately before the reproductive stage (near the dashed black line in Fig. 5).

Figure 6 compares the time series of total aboveground biomass between the simulated and experimental data. Except for Tanzania, MATCRO-Maize accurately estimated the increasing trend of total aboveground biomass towards maturity, although the simulated biomass in Brazil was underestimated at maturity. The simulated total aboveground biomass in Tanzania increased until maturity, while the observations gradually decreased towards maturity time (Fig. 6 (c)).

Figure 7 compares the 1:1 line between the simulated and experimental data for the seasonal LAI (Fig. 7 (a)), seasonal total aboveground biomass (Fig. 7 (b)), and harvested yield (Fig. 7 (c)). The LAI underestimation in France and Brazil (Fig. 5) could also be seen with a large RMSE, which is approximately 50% of the average LAI across all observational values at 3 sites except for Tanzania, although overall, the comparison was statistically significant (p value < 0.01), with a COR of 0.762. The comparison of total aboveground biomass was statistically significant (p value < 0.001), with a COR of 0.895, although the RMSE was 3,628.3 [kg ha⁻¹], which corresponds to approximately 35% of the average of all observed total aboveground biomass. While the comparison of the final crop yield was statistically significant (p value < 0.01), there was a relatively low COR compared with the LAI and total aboveground biomass due to the small sample size (N=4) and the overestimation for Tanzania. The RMSE was 2,575.0 [kg ha⁻¹], which is approximately 30% of the average observational yield at all the sites.
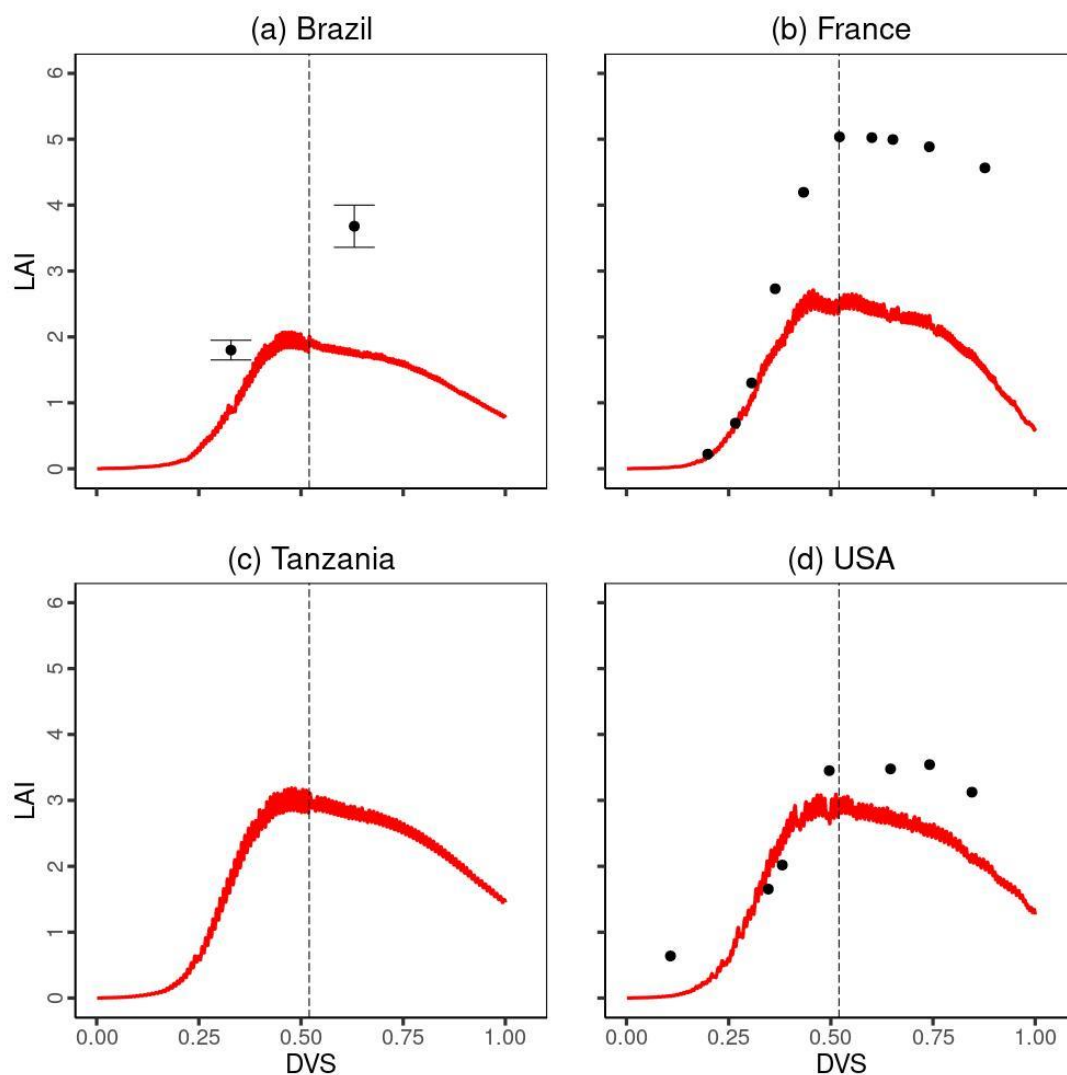
Figure 5. Temporal evaluation of leaf area index (LAI) simulated by MATCRO-Maize (red line) at each site: (a) Brazil, (b) France, (c) Tanzania and (d) the USA across the developmental stage (D_{vs}). The observation data in each site is shown by black point. Notably, there were no observational data in Tanzania. The error bars were provided only for Brazil. The dashed black line shows the flowering time.

370
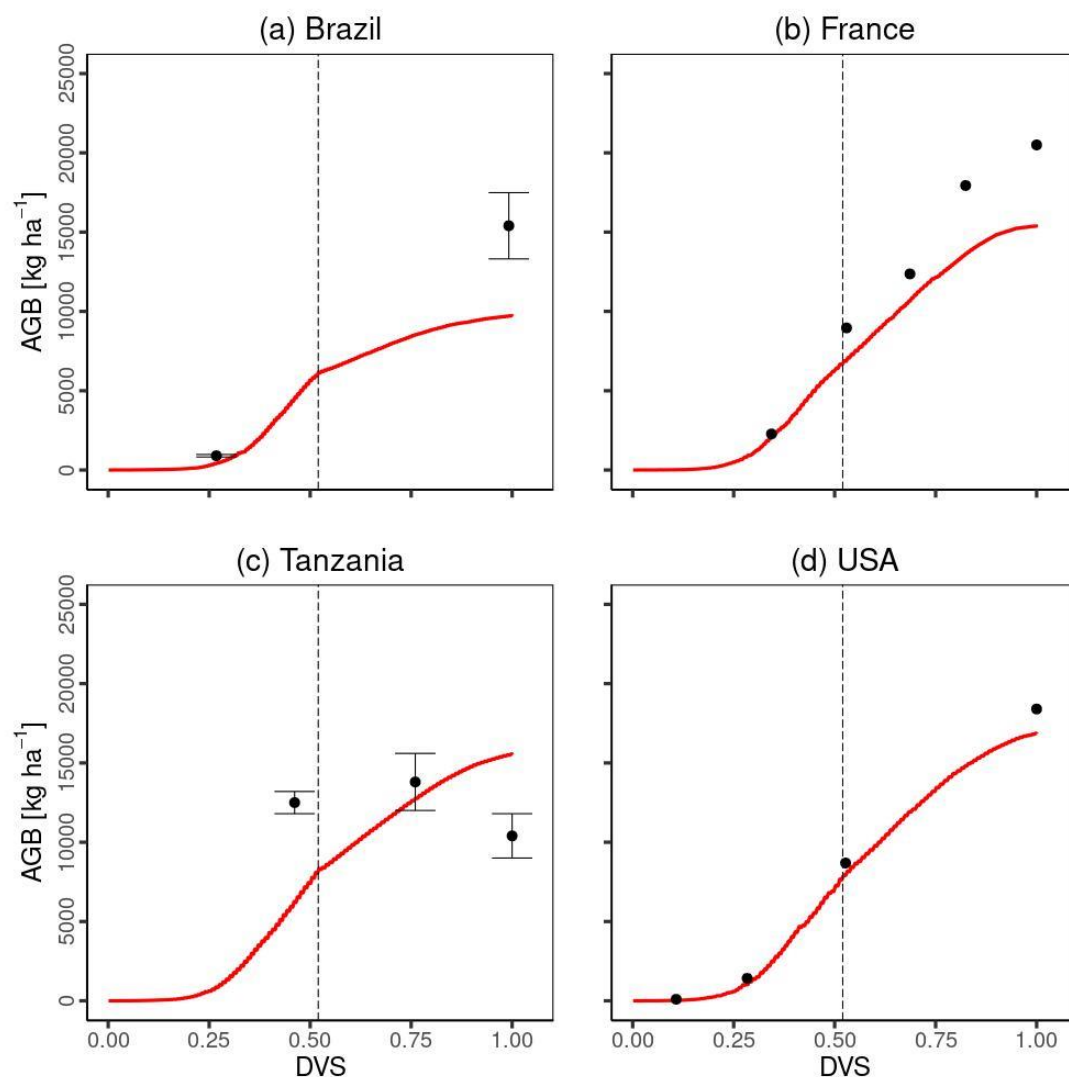
Figure 6. Temporal evaluation of total aboveground biomass (AGB) simulated by MATCRO-Maize (red line) at each site: (a) Brazil, (b) France, (c) Tanzania and (d) the USA across the developmental stage (D_{vs}). The observation data in each site is shown by black point. The error bars were only provided for Brazil and Tanzania. The dashed black line shows the flowering time.

375
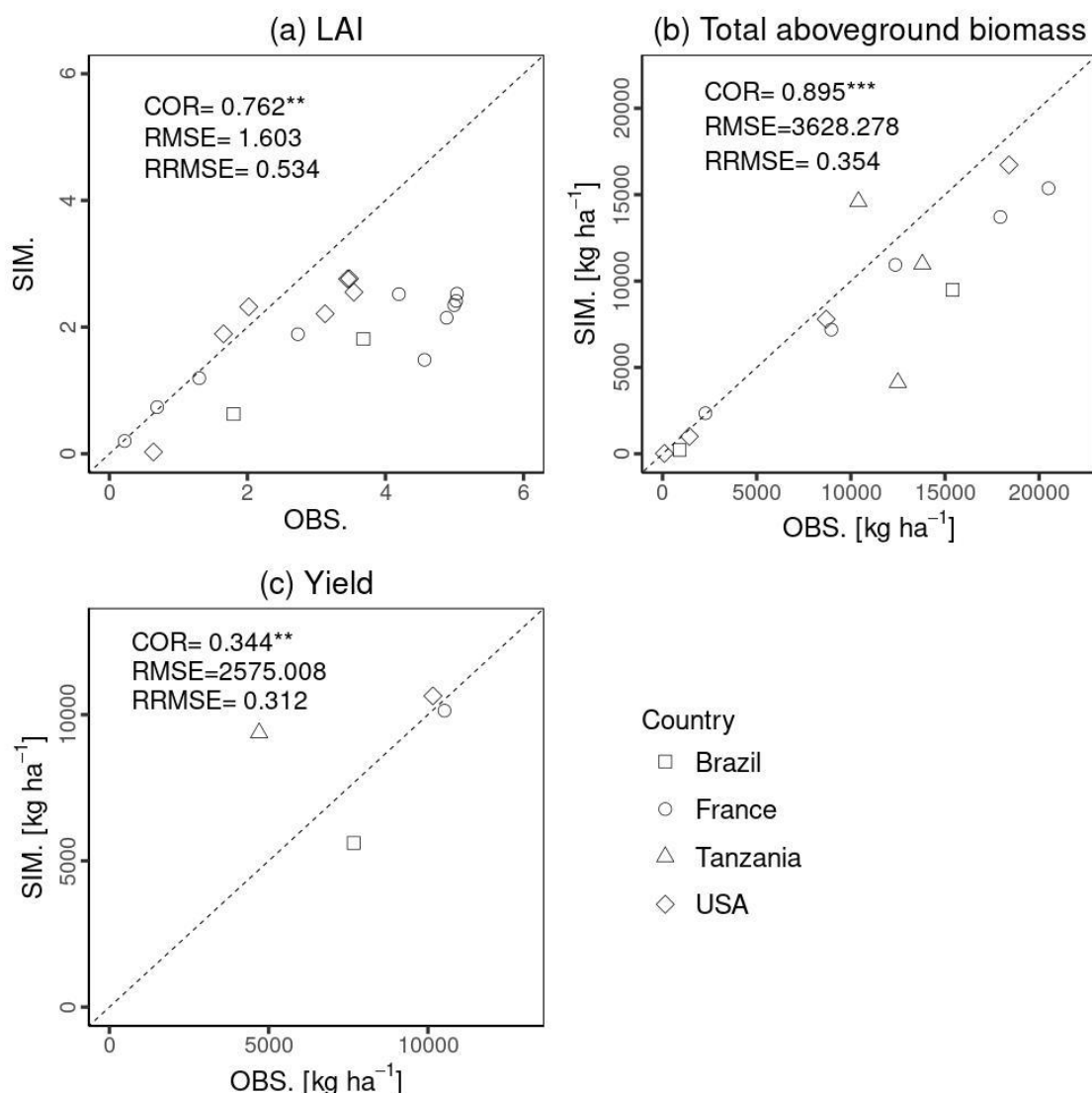
Figure 7. Statistical comparison (COR, RMSE, and RRMSE) of (a) LAI, (b) Total aboveground biomass, and (c) Yield. The x-axis (OBS) represents the observational data, and the y-axis (SIM.) is the simulated data. Shapes show each site: Brazil (square), France (circle), Tanzania (triangle), and the USA (diamond). Notably, there was no observed LAI in Tanzania. The symbols ***, **, indicate p values < 0.001 and 0.01, respectively.

3.2 Global-scale simulations

A comparison of the global distributions is shown in Figure 8 (simulation: Fig. 8(a); GDHY dataset: Fig. 8(b)). While the overestimation could be seen mainly in tropical regions, the simulated yield could capture high-yielding regions, including the Corn Belt in the United States and the northern part of China. Temporal changes in the global yield across 30 years indicated that although the global yield had an NMAE of 0.67, indicating a simulation error of 67% with respect to the
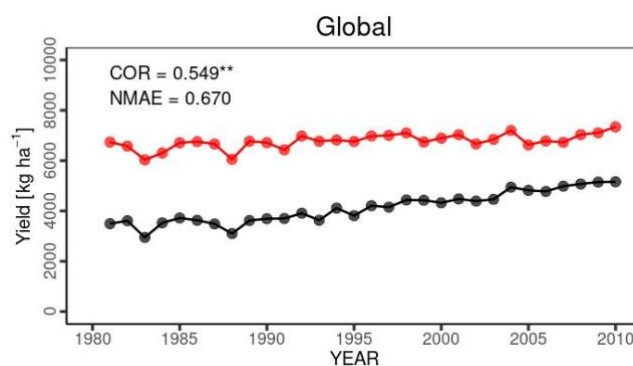
average FAO yield, the comparison of the interannual variability between the simulations and observations was statistically significant (p value < 0.01), with a COR of 0.549 (Figure 9). For the top 20 producing countries, MATCRO-Maize also tended to overestimate the yield in terms of the annual yield (Figure 10) and the average yield over a 30-year period (Figure 11). The overestimation was strong in Egypt, where the simulated yield was approximately four times greater across 30 years.
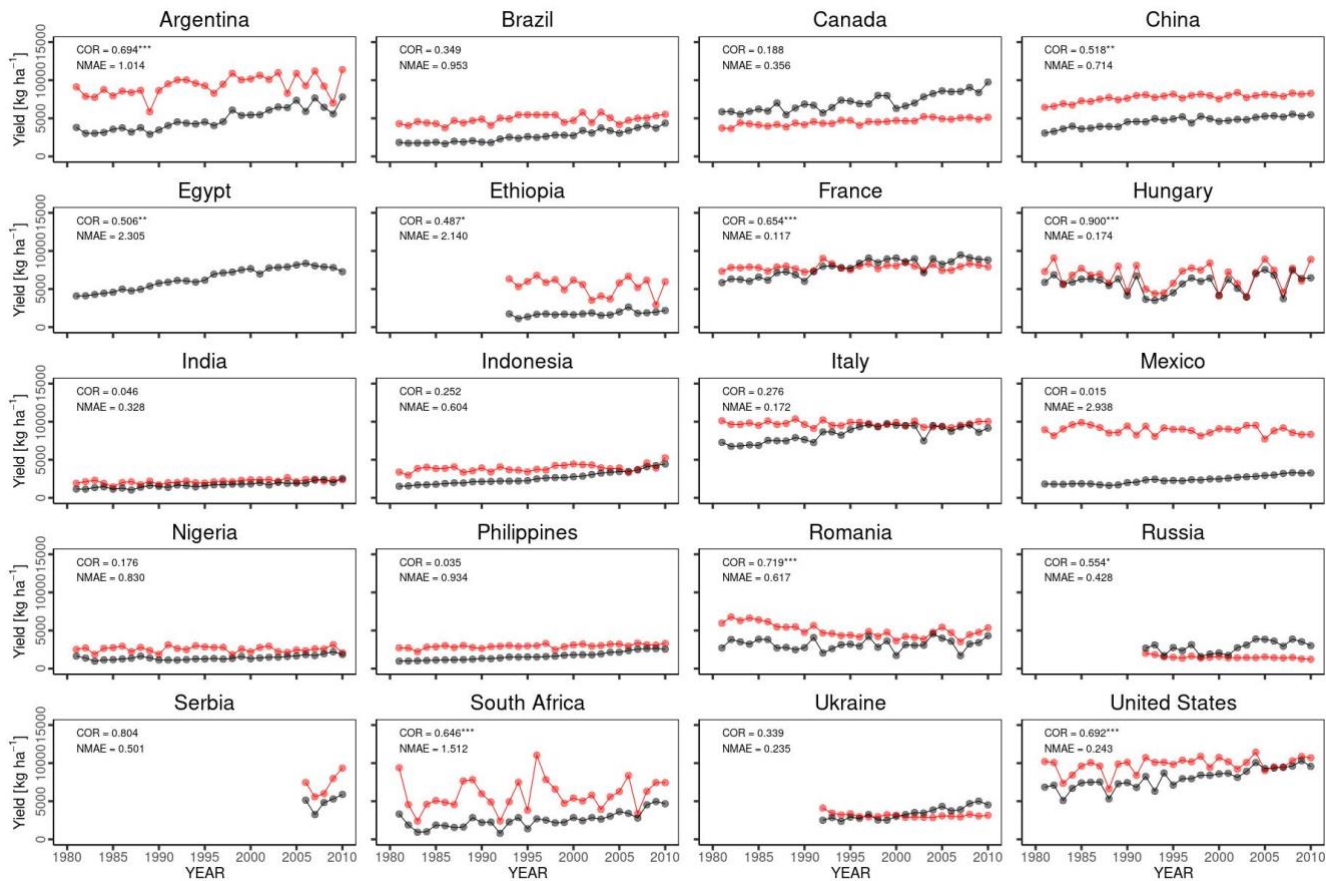
390   In terms of interannual variability, half of the 20 countries were statistically significant, with p values < 0.001 for 6 countries, < 0.01 for 2 countries, and < 0.05 for 2 countries (Fig. 10). The 30-year average comparison was also statistically significant (p value < 0.01), with a COR of 0.58, although the RMSE was 4,007.7 [kg ha^{-1}], which is almost the same as the average yield of the top 20 maize-producing countries (Fig. 11).
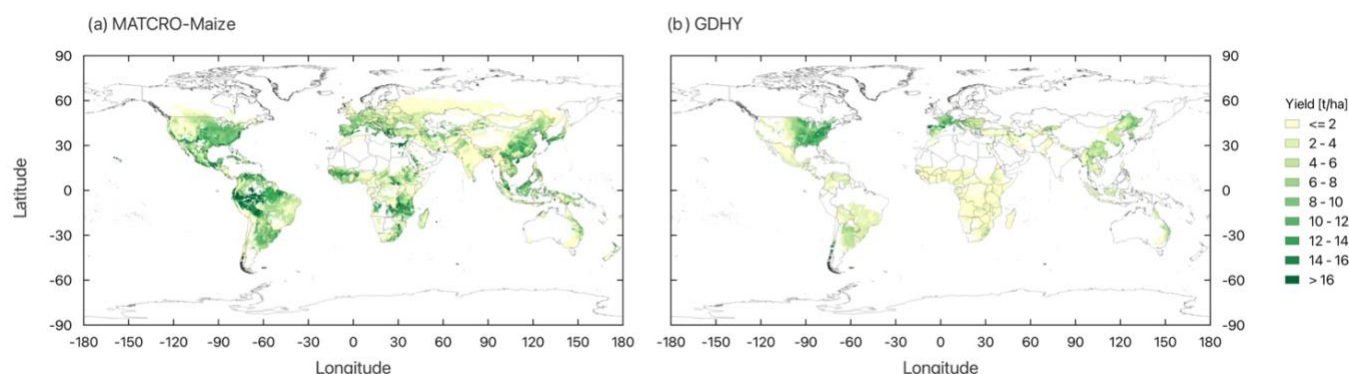

Figure 8. Global distribution of the 30-year average (1981-2010) maize yield by (a) simulations from the MATCRO-Maize and (b) the GDHY dataset. The yield is aggregated based on the harvested area from MIRCA2000.

Figure 9. Interannual variability in global maize yield from 1981 to 2010 for our simulation (red circles) and FAOSTAT (black) yields. COR represents the correlation coefficient of interannual variability. NMAE means normalized mean absolute error. Asterisks ** indicate p value < 0.01.

19

Figure 10. Comparison of interannual variability for the top 20 maize-producing countries. Similar to Fig. 9. Notably, the simulated yield in Egypt is not shown as it extends beyond the range of the y-axis. The symbols ***, **, and * indicate p values < 0.001, 0.01, and 0.05, respectively.
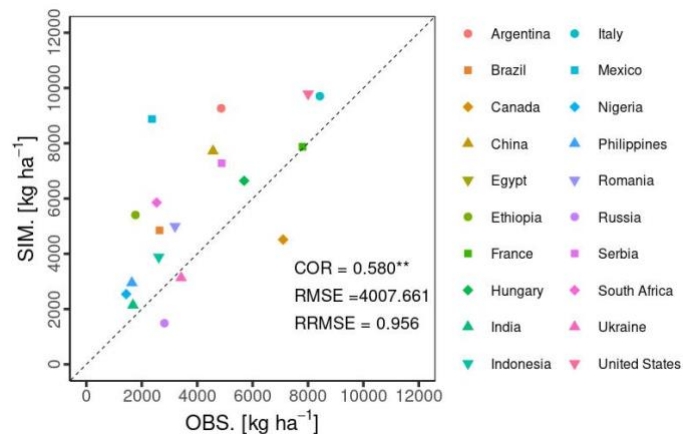
Figure 11. Accuracy of the 30-year average of the simulated yield (SIM) to the observed yield (OBS from FAOSTAT data) for the top 20 countries. Notably, the Egypt data points are not shown as exceeding the range of the y-axis. Asterisks ** indicate a p value < 0.01.

Figures 12 (a) and (b) show the comparisons based on N_{fert} for each FAOSTAT and simulated yield, respectively. MATCRO has a strong N_{fert} effect on the yield reflected in the steep slope of the regression line with relatively similar intercepts (slope: 27.6 and 47.3; intercept: 1,701.0 and 2,187.4 for FAOSTAT and MATCRO-Maize, respectively). This effect was scarcely alleviated by the intentionally changed setting (Fig. 12 (c), (d)), mainly because of the effect of Egypt as

415   an outlier. Figure 13 shows the same comparison as Fig. 12 without Egypt. The slope was similar to that of FAOSTAT (33.8 for FAOSTAT and 30.35 for MATCRO-Maize), whereas the intercept was approximately 2.5 times greater (1,310.6 for FAOSTAT and 3,247.0 for MATCRO-Maize) (Fig. 13 (a), (b)). The changed equation and parameter partly alleviated the large intercept, although the slope became slightly smaller than that of FAOSTAT (Fig. 13 (c), (d)).
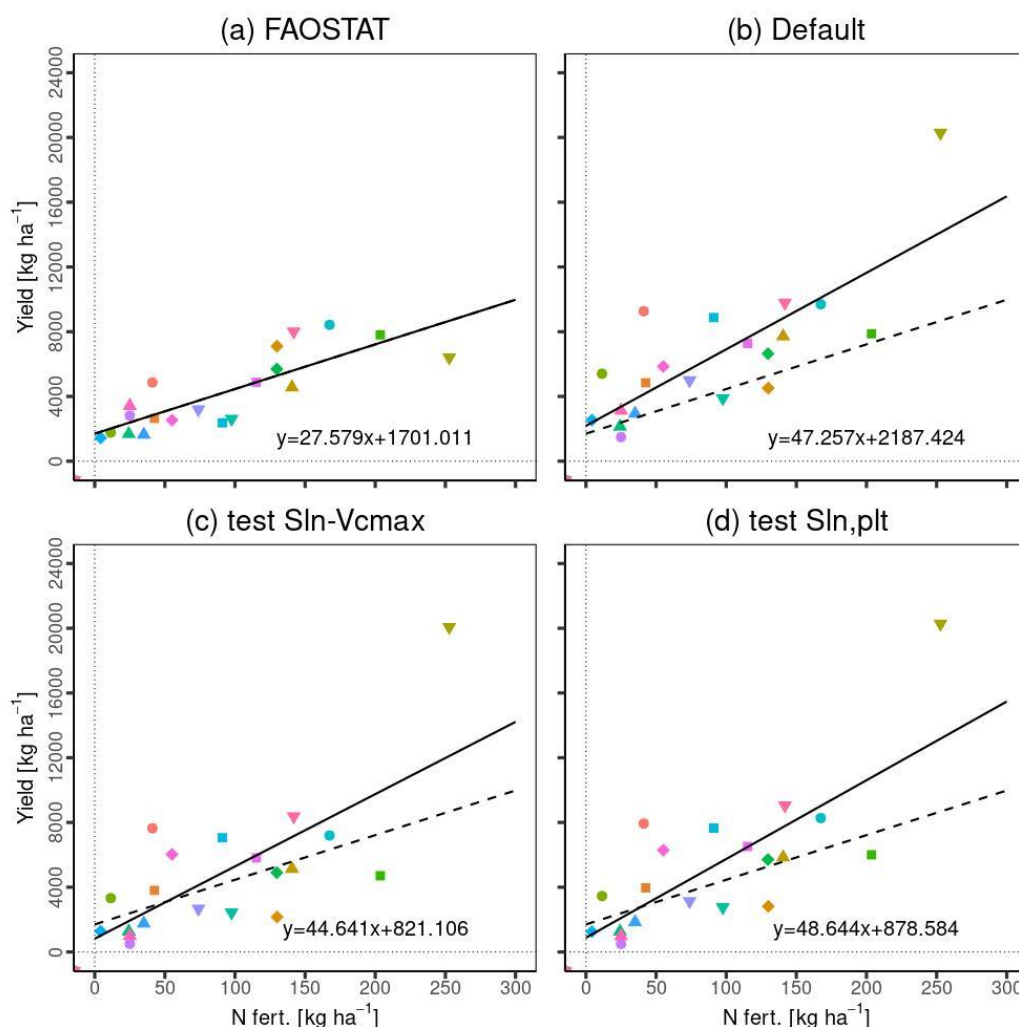
Figure 12. N_{fert} impact on yield of (a) FAOSTAT, (b) simulated yield with the original setting (Default), (c) simulated yield with the changed S_{ln}-V_{cmax} relationship (test Sln-Vcmax), (d) simulated yield with the changed parameter related to the D_{vs}-S_{ln} function (test Sln, plt). N_{fert} (N fertilizer) and country yield were averaged across 30 years for each country. The legends are the same as those in Fig. 11. The dashed lines in (b), (c), and (d) indicate the regression lines in (a).
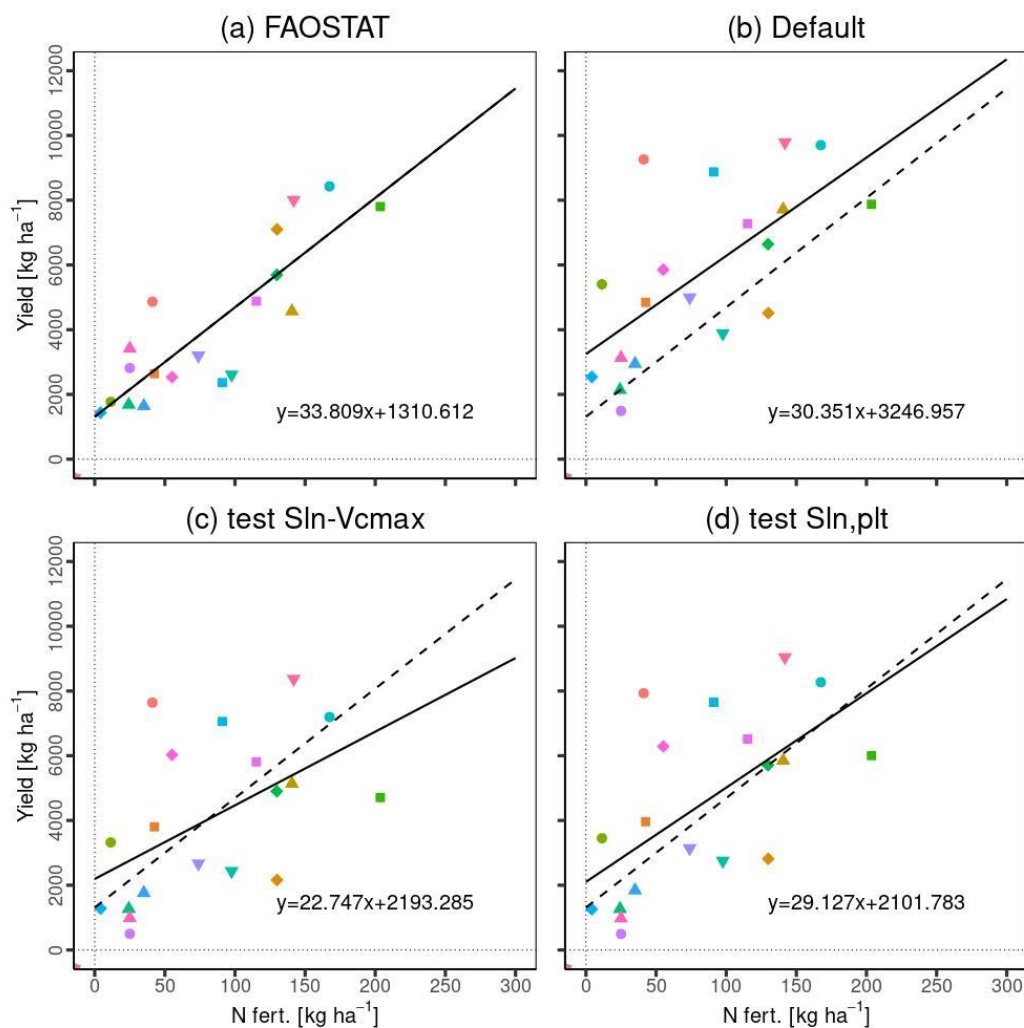
Figure 13. N_{fert} impact on yield. Similar to Fig. 12, but without Egypt.

4 Discussion

4.1 Point-scale simulations

The simulated LAI, total aboveground biomass, and harvested yield were statistically significant at the point scale (Fig. 7), indicating that the MATCRO-Maize model could simulate maize growth and yield relatively well. However, there were some discrepancies between the simulations and observations, such as the underestimation of the LAI in Brazil and France, the underestimation of the total aboveground biomass in Brazil, and the different growth trends of the total aboveground biomass in Tanzania.

The reason for the underestimation of the LAI in France might be related to the effect of plant density, which is not currently considered in MATCRO. The actual plant density [plants m^{-2}] at each site was 9.5 (France), 7.5 (USA), 6.6 (Brazil), and 9.5 (Tanzania) (Bassu et al., 2014). Some studies have shown that LAI trends are affected primarily by the plant density factor relative to N_{fert} and hybrids (Boomsma et al., 2009; Ciampitti et al., 2013a; Ciampitti and Vyn, 2011). This may be the reason for the underestimation that MATCRO could not reproduce the trends driven by plant density, although other important factors (e.g., management practices, climatic conditions), which are quite different from each site in the literature, would also affect crop growth variables, including the LAI.

Both the underestimation of the LAI and total aboveground biomass in Brazil were probably caused by the field experimental conditions of $N_{fert} = 0$, given its effect on crop growth in MATCRO. The reason for the lack of fertilization in the field experiment was that sufficient N was released by organic matter mineralization (Bassu et al., 2014), which was not considered in the model. Moreover, N_{fert} directly affects S_{ln} in MATCRO, with an increasing trend towards flowering and then a decreasing trend towards maturity (Fig. 1). S_{ln} is related to $V_{cmax25}(0)$, which in turn affects the photosynthesis calculation (Section 2.1 and Section 2.2.2). In particular, during the reproductive stage, we used Eq. (27), which results in a low $V_{cmax25}(0)$ under low S_{ln} due to the more gradual slope of the curve compared with the vegetative stage (1.41 for the reproductive stage, and 2.9 for the vegetative stage, in Eq. (27)), indirectly leading to low biomass accumulation through photosynthesis. This could be attributed to the underestimation of total aboveground biomass at maturity (Fig. 6 (a)). For underestimation of the LAI, low leaf biomass accumulation, which is derived from the same mechanism, would be the reason considering the calculation process of the LAI in MATCRO. The LAI is determined by the division of the leaf biomass weight by S_{lw}, which depends on D_{vs}. Because S_{lw} is calculated from the same parameter at all sites (Eq. (33) and Fig. 3), leaf weight is the factor that causes differences between sites, leading to the underestimation of the LAI in Brazil. Therefore, the condition of $N_{fert} = 0$ might be the reason for both underestimations.

One possible reason for the difference in the growth trend of biomass in Tanzania might be related to growing season length. The cultivar used in Tanzania was a short season type with 99 days of observed growing season length, whereas the cultivars at other sites were medium or long season type with lengths ranging from 122 to 173 days (Bassu et al., 2014). Capristo et al. (2007) reported that, compared with medium- and long-season cultivars, short-season cultivars presented the lowest biomass accumulation from flowering to maturity, which was reflected in the observed biomass (Fig. 6 (c)). This might indicate that the trend of biomass accumulation differs across growing season types, although other factors, such as climatic conditions or biotic stresses, could also affect accumulation. While MATCRO considers the growing season length as $G_{dd,m}$ to judge the harvesting time, this does not mean that MATCRO could capture the difference in trends due to growing season types, possibly leading to the gap between the simulations and observations shown in Tanzania.

4.2 Global-scale simulations

465 A comparison of the global distribution of maize yield revealed that MATCRO-Maize could capture the distribution of high-yield regions but could not capture the yield in tropical regions (Figure 8). Similar overestimations in tropical regions have also been reported in other global models, possibly because of the lack of representation of extreme weather or crop pests (Lombardozzi et al., 2020; Osborne et al., 2015).

Notably, MATCRO-Maize tended to overestimate the absolute values for both the total global yield and the yields of the top 20 countries, as reflected in the NMAE and RMSE values (Figures 9, 10, and 11). The simulated total global yield is

470 determined mainly by the yield of the top 3 maize-producing countries, the United States, China, and Brazil, which have large cultivated areas (Table 3). All three countries' yields were overestimated, where the simulated yields were approximately 1.2, 1.7, and 1.8 times greater for the 30-year averages in the United States, China, and Brazil, respectively, leading to overestimation of the total global yield. Such overestimations in the main producing countries, especially in China and Brazil, are also observed in other global crop models (Von Bloh et al., 2018; Osborne et al., 2015; Schaphoff et al.,

475 2018). This might indicate that there are factors that are important for determining yields but are not considered in most crop models.

For the top 20 producing countries, the overestimation was strong in Egypt, with an approximately fourfold greater simulated yield than that of FAOSTAT. This overestimation might be caused by the irrigated conditions in all grids in Egypt. Under manually changed rainfed conditions, crop growth in Egypt in the model was almost not simulated because of the

480 inhibited photosynthesis rate caused by strong water stress. Under irrigated conditions, this strong water stress was alleviated. In addition, the radiation in Egypt was consistently strong throughout the growing period, and N_{fert} was highest among the top 20 countries across the 30 years simulated, increasing from approximately 180 kg ha^{-1} in 1980 to 360 kg ha^{-1} in 2010. This caused the colimited photosynthesis rate to be high (Eq. (4)) across the growing seasons, leading to marked overestimation.

485 Although the simulated yield has the large error in terms of the absolute value, the comparison of the 30-year average yield was statistically significant, with a COR of 0.58 (p value < 0.01) and an RMSE of 4,008 kg ha^{-1} (Fig. 11), showing the ability to capture the spatial distribution of the yield both in low- and high-producing countries from the first perspective of the comparison (Section 2.3.2). This result was comparable with the similar result of another model: LPJ-GUESS (Olin et al., 2015), with a COR of 0.46 and an RMSE of 4,300 kg ha^{-1} (Table 4), although the targeted countries were different (top 20

490 producing countries for MATCRO-Maize, whole countries for LPJ-GUESS).

In terms of interannual variability from the second perspective, the total global yield and approximately one-third of the top 20 producing countries were statistically significant, with p values < 0.01 (Figs. 9 and 10), indicating that MATCRO-Maize could reproduce the climatic effect globally to some extent. This might also be supported by the similar comparisons of other global crop models in terms of statistics (Table 4), although it is difficult to simply compare the statistical values

495 between the models owing to the differences in periods, input data, and methods for detrending and aggregating the yield.

The COR of interannual variability for total global yield in MATCRO-Maize was in the range of those of the other models (0.55; 0.42~0.89, respectively). For the top 20 countries, almost all the COR values also ranged between those of the other models. Therefore, these comparisons from two perspectives might indicate that MATCRO-Maize could yield reasonable results.

500

Table 3. Maize cultivated land area for 20 major producer countries from MIRCA2000 (Portmann et al., 2010).

Country	Total area [ha]	Rainfed area [ha]	Irrigated area [ha]
Argentina	3,248,715.9	3,147,580.7	101,135.3
Brazil	11,223,262.5	11,120,154.9	103,107.6
Canada	1,364,585.3	1,328,206.2	36,379.1
China	24,376,805.2	11,615,190.0	12,761,615.2
Egypt	827,766.1	0.0	827,766.1
Ethiopia	1,172,231.1	1,084,795.6	87,435.5
France	3,128,401.0	2,257,380.0	871,021.0
Hungary	1,057,610.7	1,052,622.6	4,988.1
India	6,294,770.9	4,833,685.9	1,461,085.0
Indonesia	3,479,825.7	3,135,443.9	344,381.8
Italy	1,322,692.9	534,281.4	788,411.5
Mexico	7,459,039.5	5,852,617.4	1,606,422.1
Nigeria	3,686,757.3	3,667,564.5	19,192.8
Philippines	2,590,081.0	2,590,081.0	0.0
Romania	3,139,981.1	3,016,990.5	122,990.6
Russia	4,206,747.0	3,594,403.2	612,343.9
Serbia	1,074,614.2	1,062,985.8	11,628.4
South Africa	3,060,053.5	2,930,208.2	129,845.4
Ukraine	3,382,783.5	3,194,146.2	188,637.3
United States	31,307,667.3	26,508,600.7	4,799,066.7

505

510

515

520

Table 4. Statics of model simulation accuracy of the MATCRO-Maize and other crop models. Notably, the asterisks for GGCMI phase I indicate the p values: *** for p values < 0.001, ** for p values < 0.05, * for p values < 0.1, whereas those of LPJmL4 and MATCRO-Maize indicate the p values: *** for p values < 0.001, ** for p values < 0.01, * for p values < 0.05.

	References	Period	COR of interannual variability						
			Global	USA	China	Brazil	Mexico	France	Argentina
MATCRO-Maize	-	1981–2010	0.549**	0.692***	0.518**	0.349	0.015	0.654***	0.694***
JULES-crop[1]	Osborne et al., 2015	1961–2008	0.48	0.43	0.12	0.12	0.061	0.52	0.57
LPJmL4[2]	Schaphoff et al., 2018	1981–2010	–	0.675***	0.676***	0.169	-0.124	-0.331	0.717***
LPJmL5[3]	Bloh et al., 2018	1981–2010	–	0.686***	0.641***	0.0591	0.0618	0.461*	0.650***
GGCMI phase 3[4]	Jägermeyr et al., 2021	1981–2015	–	0.817	0.245	0.029	–	0.649	0.727
GGCMI phase 1[5]	Müller et al., 2017	1982–2006	0.42**~0.89***	0.89	0.75	0.66	0.85	0.87	0.85

	References	Period	COR of interannual variability						
			Romania	South Africa	India	Italy	Hungary	Indonesia	Ukraine
MATCRO-Maize	-	1981–2010	0.719***	0.646***	0.046	0.276	0.900***	0.252	0.339
JULES-crop[1]	Osborne et al., 2015	1961–2008	0.32	0.41	0.34	0.34	0.33	0.065	–
LPJmL4[2]	Schaphoff et al., 2018	1981–2010	–	0.711***	-0.22	–	–	0.124	-0.046
LPJmL5[3]	Bloh et al., 2018	1981–2010	–	0.667***	0.496**	–	–	-0.163	0.152
GGCMI phase 3[4]	Jägermeyr et al., 2021	1981–2015	–	–	–	–	–	–	–
GGCMI phase 1[5]	Müller et al., 2017	1982–2006	0.90	0.91	0.76	0.76	0.90	0.42	0.61

	References	Period	30-year averaged yield	
			COR	RMSE [kg ha^{-1}]
MATCRO-Maize	-	1981–2010	0.580**	4,008
LPJ-GUESS[6]	Olin et al., 2015	1996–2005	0.46	4,300

[1] Countries-level comparison was conducted for 12 countries, which were detrended only for observation. p values are not shown.

[2,3] Countries-level comparison was conducted for the top 10 producing countries, which were detrended via a 5-year moving average.

[4] Twelve global gridded crop models were used. The COR shown here is the ensembled mean value for the 5 largest producing countries after detrending. p values are not shown.

[5] Fourteen global gridded crop models were used. The COR of the global yield shown here is the minimum and maximum value, except for one nonsignificant correlation with the default setting. The COR of each country is the best correlation among the 14 models, including 3 different settings with statistical significance (p values are not shown). For both the global and country-level comparisons, a 5-year moving average was used to remove trends.

[6] The 10-year average comparisons included all countries. p values are not shown.

4.3 Model limitations

535 The limitation of the current MATCRO-Maize is the strong N_{fert} effect shown in the validation (the site in Brazil for the point scale) and comparison based on the N_{fert} (Figures 12 and 13). In the model, N_{fert} has the direct relationship with S_{ln} (Eq. (28)) and consequently affects $V_{cmax25}(0)$ through the function S_{ln}-$V_{cmax25}(0)$ (Eq. (27)). Therefore, the strong N_{fert} effect is caused by either the former, the latter, or both processes. Few studies have explicitly shown time series changes in S_{ln} and S_{ln}-V_{cmax} relationships from experiments. We used some of them to establish the functions shown in Eqs. (27) and

540 (28) (Section 2.2.2) at this stage, resulting in a strong N_{fert} effect in the model. However, the intentional experiment indicated that the changed relationships could partly reproduce the adequate effect, which was observed in the FAOSTAT yield. This might mean that the established functions include a degree of uncertainty, and if we establish robust relationships based on other experimental data under more comprehensive conditions, it might be possible to improve the model in terms of the N_{fert} effect, leading to a more accurate simulation of maize yield.

545 In this study, we applied identical parameters to simulate the global yield across all grid cells and throughout the years without considering cultivar differences. As mentioned in Section 3.1.2, the trend of biomass accumulation would differ across growing season types. Moreover, in major producing countries, such as the United States and China, some studies have shown that there is genetic gain in terms of maize yield (Cooper et al., 2014; Duvick et al., 2003; Liu et al., 2021). Such cultivar differences and long-term genetic improvements are not included in the current MATCRO-Maize. This finding

550 indicates that the generic parameterization used in the model would be simple in accounting for the diversity of crop cultivars (Lombardozzi et al., 2020), partly leading to a gap between the simulations and observations, which is recognized as a limitation of the global model (Osborne et al., 2015).

In addition, other important factors that are not considered in the current MATCRO also affect crop growth and final yield. These factors include biotic stresses (e.g., diseases, pests) and detailed management practices (e.g., plant density, as

555 mentioned in Section 4.1). Further improvement to incorporate such factors with reliable N_{fert}-related functions could be needed to contribute to more accurate simulations and contribute to studies on the interaction between climate and agriculture.

5 Conclusions

We developed a process-based crop model for maize yield estimation, called MATCRO-Maize, by incorporating C4 leaf-

560 level photosynthesis and some crop-specific parameters into MATCRO. The model was first validated at the point scale, showing a somewhat reasonable accuracy considered with insufficient field-based information for parameterization. The calibrated parameters were set from point-scale experimental data and used uniformly in the global-scale simulation. MATCRO-Maize could represent the spatial distribution well and showed reasonable responses to climatic variability, where the results were comparable with those of other studies in terms of statistics. The strong nitrogen fertilizer effect was one of

565 the MATCRO limitations, while the established functions related to nitrogen fertilizer in the model have a degree of uncertainty. Further experimental data under more comprehensive conditions might improve the model. Overall, MATCRO-Maize could contribute to climate effect studies through its ability to be integrated with the LSM for crop growth and the interactions between climate and agriculture.

Code and data availability.

570 The source code used in this study is archived at https://doi.org/10.5281/zenodo.14869445 (Nagata et al., 2025).

Author contributions.

TK supervised this study and acquired the funding. YM developed the model source code and supervised this study. MN adjusted the source code for this study, performed the model simulations, and analysed the model output. MN prepared the original draft, which was supervised by TK, YM, and AY. The final manuscript was written by MN and approved by all the
575 authors.

Acknowledgements.

References

Allen R.G., Pereira L.S., Raes D., and Smith M.: Crop Evapotranspiration: Guidelines for Computing Crop Water
585   Requirements - FAO Irrigation and drainage paper 56, FAO - Food and Agriculture Organization of the United Nations, Rome, 1998.

Asseng, S., Ewert, F., Rosenzweig, C., Jones, J. W., Hatfield, J. L., Ruane, A. C., Boote, K. J., Thorburn, P. J., Rötter, R. P., Cammarano, D., Brisson, N., Basso, B., Martre, P., Aggarwal, P. K., Angulo, C., Bertuzzi, P., Biernath, C., Challinor, A. J., Doltra, J., Gayler, S., Goldberg, R., Grant, R., Heng, L., Hooker, J., Hunt, L. A., Ingwersen, J., Izaurralde, R. C.,
590   Kersebaum, K. C., Müller, C., Naresh Kumar, S., Nendel, C., O'Leary, G., Olesen, J. E., Osborne, T. M., Palosuo, T., Priesack, E., Ripoche, D., Semenov, M. A., Shcherbak, I., Steduto, P., Stöckle, C., Stratonovitch, P., Streck, T., Supit, I.,

Tao, F., Travasso, M., Waha, K., Wallach, D., White, J. W., Williams, J. R., and Wolf, J.: Uncertainty in simulating wheat yields under climate change, Nat Clim Chang, 3, 827–832, https://doi.org/10.1038/NCLIMATE1916, 2013.

Ball J.T: An analysis of Stomatal Conductance, Stanford University, CA, USA, 1988.

595 Bassu, S., Brisson, N., Durand, J. L., Boote, K., Lizaso, J., Jones, J. W., Rosenzweig, C., Ruane, A. C., Adam, M., Baron, C., Basso, B., Biernath, C., Boogaard, H., Conijn, S., Corbeels, M., Deryng, D., De Sanctis, G., Gayler, S., Grassini, P., Hatfield, J., Hoek, S., Izaurralde, C., Jongschaap, R., Kemanian, A. R., Kersebaum, K. C., Kim, S. H., Kumar, N. S., Makowski, D., Müller, C., Nendel, C., Priesack, E., Pravia, M. V., Sau, F., Shcherbak, I., Tao, F., Teixeira, E., Timlin, D., and Waha, K.: How do various maize crop models vary in their responses to climate change factors?, Glob Chang

600 Biol, 20, 2301–2320, https://doi.org/10.1111/gcb.12520, 2014.

Von Bloh, W., Schaphoff, S., Müller, C., Rolinski, S., Waha, K., and Zaehle, S.: Implementing the nitrogen cycle into the dynamic global vegetation, hydrology, and crop growth model LPJmL (version 5.0), Geosci Model Dev, 11, 2789–2812, https://doi.org/10.5194/gmd-11-2789-2018, 2018.

Bonan, G. B., Lawrence, P. J., Oleson, K. W., Levis, S., Jung, M., Reichstein, M., Lawrence, D. M., and Swenson, S. C.:

605 Improving canopy processes in the Community Land Model version 4 (CLM4) using global flux fields empirically inferred from FLUXNET data, J Geophys Res, 116, 1–22, https://doi.org/10.1029/2010JG001593, 2011.

Bondeau, A., Smith, P. C., Zaehle, S., Schaphoff, S., Lucht, W., Cramer, W., Gerten, D., Lotze-campen, H., Müller, C., Reichstein, M., and Smith, B.: Modelling the role of agriculture for the 20th century global terrestrial carbon balance, Glob Chang Biol, 13, 679–706, https://doi.org/10.1111/J.1365-2486.2006.01305.X, 2007.

610 Boomsma, C. R., Santini, J. B., Tollenaar, M., and Vyn, T. J.: Maize Morphophysiological Responses to Intense Crowding and Low Nitrogen Availability: An Analysis and Review, Agron J, 101, 1426–1452, https://doi.org/10.2134/AGRONJ2009.0082, 2009.

Bouman, B. A. M., Kropff, M., Tuong, T., Wopereis, M., ten Berge, H., and van Laar, H.: Oryza2000: modeling lowland rice, International Rice Research Institute, and Wageningen: Wageningen University and Research Centre, Philippines

615 and Wageningen, the Netherlands, 235 pp., 2001.

Büchner, M. and Reyer, P. O. , C.: ISIMIP3a atmospheric composition input data (v1.2). ISIMIP Repository., https://doi.org/https://doi.org/10.48364/ISIMIP.664235.2, 2022.

Campbell, G. S. and Norman, J. M.: An Introduction to Environmental Biophysics, Springer New York, NY, New York, USA, https://doi.org/10.1007/978-1-4612-1626-1, 1998.

620 Capristo, P. R., Rizzalli, R. H., and Andrade, F. H.: Ecophysiological Yield Components of Maize Hybrids with Contrasting Maturity, Agronomy Jornal, 99, 1111–1118, https://doi.org/10.2134/agronj2006.0360, 2007.

Ciampitti, I. A. and Vyn, T. J.: A comprehensive study of plant density consequences on nitrogen uptake dynamics of maize plants from vegetative to reproductive stages, Field Crops Res, 121, 2–18, https://doi.org/10.1016/J.FCR.2010.10.009, 2011.

625   Ciampitti, I. A., Murrell, S. T., Camberato, J. J., Tuinstra, M., Xia, Y., Friedemann, P., and Vyn, T. J.: Physiological dynamics of maize nitrogen uptake and partitioning in response to plant density and N stress factors: I. Vegetative phase, Crop Sci, 53, 2105–2119, https://doi.org/10.2135/cropsci2013.01.0040, 2013a.

Ciampitti, I. A., Murrell, S. T., Camberato, J. J., Tuinstra, M., Xia, Y., Friedemann, P., and Vyn, T. J.: Physiological dynamics of maize nitrogen uptake and partitioning in response to plant density and nitrogen stress factors: II.
630   reproductive phase, Crop Sci, 53, 2588–2602, https://doi.org/10.2135/cropsci2013.01.0041, 2013b.

Collatz, G., Ribas-Carbo, M., and Berry, J.: Coupled Photosynthesis-Stomatal Conductance Model for Leaves of C4 Plants, Functional Plant Biology, 19, 519, https://doi.org/10.1071/PP9920519, 1992.

Collatz, G. J., Ball, J. T., Grivet, C., and Berry, J. A.: Physiological and environmental regulation of stomatal conductance, photosynthesis and transpiration: a model that includes a laminar boundary layer, Agric For Meteorol, 54, 107–136,
635   https://doi.org/10.1016/0168-1923(91)90002-8, 1991.

Cooper, M., Gho, C., Leafgren, R., Tang, T., and Messina, C.: Breeding drought-tolerant maize hybrids for the US corn-belt: discovery to product, J Exp Bot, 65, 6191–6204, https://doi.org/10.1093/jxb/eru064, 2014.

Dai, Y., Dickinson, R. E., and Wang, Y. P.: A two-big-leaf model for canopy temperature, photosynthesis, and stomatal conductance, J Clim, 17, 2281–2299, https://doi.org/10.1175/1520-0442(2004)017<2281:ATMFCT>2.0.CO;2, 2004.

640   Drouet, J. L. and Bonhomme, R.: Effect of 3D Nitrogen, Dry Mass per Area and Local Irradiance on Canopy Photosynthesis Within Leaves of Contrasted Heterogeneous Maize Crops, Ann Bot, 93, 699–710, https://doi.org/10.1093/aob/mch099, 2004.

Duvick, D. N., Smith, J. S. C., and Cooper, M.: Long-Term Selection in a Commercial Hybrid Maize Breeding Program, in: Plant Breeding Reviews, Wiley, 109–151, https://doi.org/10.1002/9780470650288.ch4, 2003.

645   FAO: Agricultural production statistics 2000–2021, FAO, Rome, Italy, https://doi.org/10.4060/cc3751en, 2022.

FAOSTAT Production / Crops and livestock products - Metadata: https://www.fao.org/faostat/en/#data/QCL/metadata, last access: 31 December 2024.

Hajima, T., Watanabe, M., Yamamoto, A., Tatebe, H., Noguchi, M. A., Abe, M., Ohgaito, R., Ito, A., Yamazaki, D., Okajima, H., Ito, A., Takata, K., Ogochi, K., Watanabe, S., and Kawamiya, M.: Development of the MIROC-ES2L Earth
650   system model and the evaluation of biogeochemical processes and feedbacks, Geosci Model Dev, 13, 2197–2244, https://doi.org/10.5194/GMD-13-2197-2020, 2020.

Iizumi, T.: Global dataset of historical yields v1.2 and v1.3 aligned version [dataset]., PANGAEA, https://doi.org/https://doi.org/10.1594/PANGAEA.909132, 2019.

Iizumi, T., Masaki, Y., Takimoto, T., and Masutomi, Y.: Aligning the harvesting year in global gridded crop model
655   simulations with that in census reports is pivotal to national-level model performance evaluations for rice, European Journal of Agronomy, 130, 126367, https://doi.org/10.1016/J.EJA.2021.126367, 2021.

Intergovernmental Panel on Climate Change (IPCC): Technical Summary, in: Climate Change 2022 – Impacts, Adaptation and Vulnerability, Cambridge University Press, 37–118, https://doi.org/10.1017/9781009325844.002, 2023.

Jägermeyr, J., Müller, C., Ruane, A. C., Elliott, J., Balkovic, J., Castillo, O., Faye, B., Foster, I., Folberth, C., Franke, J. A.,
660   Fuchs, K., Guarin, J. R., Heinke, J., Hoogenboom, G., Iizumi, T., Jain, A. K., Kelly, D., Khabarov, N., Lange, S., Lin, T.
S., Liu, W., Mialyk, O., Minoli, S., Moyer, E. J., Okada, M., Phillips, M., Porter, C., Rabin, S. S., Scheer, C., Schneider,
J. M., Schyns, J. F., Skalsky, R., Smerald, A., Stella, T., Stephens, H., Webber, H., Zabel, F., and Rosenzweig, C.:
Climate impacts on global agriculture emerge earlier in new generation of climate and crop models, Nat Food, 2, 873–
885, https://doi.org/10.1038/s43016-021-00400-y, 2021.

665   Kanai, R. and Edwards, G. E.: The Biochemistry of C 4 Photosynthesis, in: C4 plant biology, Elsevier, 49–87, 1999.

Kinose, Y. and Masutomi, Y.: Impact Assessment of Climate Change on Rice Yield Using a Crop Growth Model and
Activities Toward Adaptation: Targeting Three Provinces in Indonesia, in: Adaptation to Climate Change in Agriculture:
Research and Practices, Springer, Singapore, 67–80, https://doi.org/10.1007/978-981-13-9235-1_5, 2019.

Kinose, Y., Masutomi, Y., Shiotsu, F., Hayashi, K., Ogawada, D., Gomez-Garcia, M., Matsumura, A., Takahashi, K., and
670   Fukushi, K.: Impact assessment of climate change on the major rice cultivar ciherang in Indonesia, Journal of
Agricultural Meteorology, 76, 19–28, https://doi.org/10.2480/agrmet.D-19-00045, 2020.

Knapp, A. K. and Medina, E.: Success of C4 photosynthesis in the Field; Lessons from Communities Dominated by C4
plants, in: C4 plant biology, Elsevier, 251–277, 1999.

Lange, S., Mengel, M., Treu, S., and Büchner, M.: ISIMIP3a atmospheric climate input data (v1.0). ISIMIP Repository.,
675   https://doi.org/10.48364/ISIMIP.982724, 2022.

Lawrence D., Fisher R., Koven C., Oleson K., Swenson S., and Vertenstein M: Technical Description of Version 5.0 of the
Community Land Model (CLM)., NCAR, 2020.

Levis, S., Gordon, B. B., Erik Kluzek, Thornton, P. E., Jones, A., Sacks, W. J., and Kucharik, C. J.: Interactive Crop
Management in the Community Earth System Model (CESM1): Seasonal influences on land-atmosphere fluxes, J Clim,
680   25, 4839–4859, https://doi.org/10.1175/JCLI-D-11-00446.1, 2012.

Lin, T., Song, Y., Lawrence, P., Kheshgi, H. S., and Jain, A. K.: Worldwide Maize and Soybean Yield Response to
Environmental and Management Factors Over the 20th and 21st Centuries, J Geophys Res Biogeosci, 126, 1–21,
https://doi.org/10.1029/2021JG006304, 2021.

Liu, G., Yang, H., Xie, R., Yang, Y., Liu, W., Guo, X., Xue, J., Ming, B., Wang, K., Hou, P., and Li, S.: Genetic gains in
685   maize yield and related traits for high-yielding cultivars released during 1980s to 2010s in China, Field Crops Res, 270,
108223, https://doi.org/10.1016/j.fcr.2021.108223, 2021.

Lombardozzi, D. L., Lu, Y., Lawrence, P. J., Lawrence, D. M., Swenson, S., Oleson, K. W., Wieder, W. R., and Ainsworth,
E. A.: Simulating Agriculture in the Community Land Model Version 5, J Geophys Res Biogeosci, 125, 1–19,
https://doi.org/10.1029/2019JG005529, 2020.

690   Long, S. P.: Environmental Responses, in: C4 plant biology, Elsevier, 12–21, 1999.

Maruyama, A. and Kuwagata, T.: Coupling land surface and crop growth models to estimate the effects of changes in the growing season on energy balance and water use of rice paddies, Agric For Meteorol, 150, 919–930, https://doi.org/10.1016/J.AGRFORMET.2010.02.011, 2010.

Masutomi, Y.: The appropriate analytical solution for coupled leaf photosynthesis and stomatal conductance models for C3 plants, Ecol Modell, 481, 110306, https://doi.org/10.1016/j.ecolmodel.2023.110306, 2023.

Masutomi, Y., Ono, K., Mano, M., Maruyama, A., and Miyata, A.: A land surface model combined with a crop growth model for paddy rice (MATCRO-Rice v. 1) - Part 1: Model description, Geosci Model Dev, 9, 4133–4154, https://doi.org/10.5194/gmd-9-4133-2016, 2016a.

Masutomi, Y., Ono, K., Takimoto, T., Mano, M., Maruyama, A., and Miyata, A.: A land surface model combined with a crop growth model for paddy rice (MATCRO-Rice v. 1) - Part 2: Model validation, Geosci Model Dev, 9, 4155–4167, https://doi.org/10.5194/gmd-9-4155-2016, 2016b.

Muchow, R. C.: Effect of nitrogen supply on the comparative productivity of maize and sorghum in a semi-arid tropical environment I. Leaf growth and leaf nitrogen, Field Crops Res, 18, 1–16, https://doi.org/10.1016/0378-4290(88)90055-X, 1988.

Muchow, R. C. and Sinclair, T. R.: Nitrogen response of leaf photosynthesis and canopy radiation use efficiency in field-grown maize and sorghum, Crop Sci, 34, 721–727, https://doi.org/10.2135/CROPSCI1994.0011183X003400030022X, 1994.

Nagata, M., Yusara, A., Kato, T., and Masutomi, Y.: Development of global maize production model MATCRO-Maize version 1.0 (MATCRO-Maize ver1.0) , Zenodo [code and dataset], https://doi.org/10.5281/zenodo.14869444, 2025.

Oleson, K. W., Lead, D. M. L., Bonan, G. B., Drewniak, B., Huang, M., Koven, C. D., Levis, S., Li, F., Riley, W. J., Subin, Z. M., Swenson, S. C., Thornton, P. E., Bozbiyik, A., Fisher, R., Heald, C. L., Kluzek, E., Lamarque, J.-F., Lawrence, P. J., Leung, L. R., Lipscomb, W., Muszala, S., Ricciuto, D. M., Sacks, W., Sun, Y., Tang, J., and Yang, Z.-L.: Technical Description of version 4.5 of the Community Land Model (CLM) Coordinating Lead Authors, NCAR, 2013.

Olin, S., Lindeskog, M., Pugh, T. A. M., Schurgers, G., Wärlind, D., Mishurov, M., Zaehle, S., Stocker, B. D., Smith, B., and Arneth, A.: Soil carbon management in large-scale Earth system modelling: Implications for crop yields and nitrogen leaching, Earth System Dynamics, 6, 745–768, https://doi.org/10.5194/ESD-6-745-2015, 2015.

Osborne, T., Slingo, J., Lawrence, D., and Wheeler, T.: Examining the interaction of growing crops with local climate using a coupled crop-climate model, J Clim, 22, 1393–1411, https://doi.org/10.1175/2008JCLI2494.1, 2009.

Osborne, T., Gornall, J., Hooker, J., Williams, K., Wiltshire, A., Betts, R., and Wheeler, T.: JULES-crop: a parametrisation of crops in the Joint UK Land Environment Simulator, Geosci. Model Dev, 8, 1139–1155, https://doi.org/10.5194/gmd-8-1139-2015, 2015.

Paponov, I. A. and Engels, C.: Effect of nitrogen supply on leaf traits related to photosynthesis during grain filling in two maize genotypes with different N efficiency, Journal of Plant Nutrition and Soil Science, 166, 756–763, https://doi.org/10.1002/jpln.200320339, 2003.

725   Paponov, I. A., Sambo, P., Erley, G. S. auf'm., Presterl, T., Geiger, H. H., and Engels, C.: Grain yield and kernel weight of two maize genotypes differing in nitrogen use efficiency at various levels of nitrogen and carbohydrate availability during flowering and grain filling, Plant Soil, 272, 111–123, https://doi.org/10.1007/s11104-004-4211-7, 2005.

Peng, B., Guan, K., Chen, M., Lawrence, D. M., Pokhrel, Y., Suyker, A., Arkebauer, T., and Lu, Y.: Improving maize growth processes in the community land model: Implementation and evaluation, Agric For Meteorol, 250–251, 64–89,
730   https://doi.org/10.1016/j.agrformet.2017.11.012, 2018.

Penning de Vries, F. W. T., Jansen, D. M., ten Berge, H. F. M., and Bakema, A.: Simulation of ecophysiological process of growth in several annual crops, Centre for Agricultural Publishing and Documentation (Pudoc), Wageningen, the Netherlands, 1989.

Portmann, F. T., Siebert, S., and Döll, P.: MIRCA2000—Global monthly irrigated and rainfed crop areas around the year
735   2000: A new high-resolution data set for agricultural and hydrological modeling, Global Biogeochem Cycles, 24, GB1011, https://doi.org/10.1029/2008GB003435, 2010.

Rienecker, M. M., Suarez, M. J., Gelaro, R., Todling, R., Bacmeister, J., Liu, E., Bosilovich, M. G., Schubert, S. D., Takacs, L., Kim, G. K., Bloom, S., Chen, J., Collins, D., Conaty, A., Da Silva, A., Gu, W., Joiner, J., Koster, R. D., Lucchesi, R., Molod, A., Owens, T., Pawson, S., Pegion, P., Redder, C. R., Reichle, R., Robertson, F. R., Ruddick, A. G., Sienkiewicz,
740   M., and Woollen, J.: MERRA: NASA's modern-era retrospective analysis for research and applications, J Clim, 24, 3624–3648, https://doi.org/10.1175/JCLI-D-11-00015.1, 2011.

Sage, R. F.: Why C4 photosynthesis?, in: C4 plant biology, Elsevier, 3–16, 1999.

Schaphoff, S., Forkel, M., Müller, C., Knauer, J., Von Bloh, W., Gerten, D., Jägermeyr, J., Lucht, W., Rammig, A., Thonicke, K., and Waha, K.: LPJmL4 - A dynamic global vegetation model with managed land - Part 2: Model
745   evaluation, Geosci Model Dev, 11, 1377–1403, https://doi.org/10.5194/gmd-11-1377-2018, 2018.

Sellers, P. J., Randall, D. A., Collatz, G. J., Berry, J. A., Field, C. B., Dazlich, D. A., Zhang, C., Collelo, G. D., and Bounoua, L.: A Revised Land Surface Parameterization (SiB2) for Atmospheric GCMS. Part I: Model Formulation, J Clim, 9, 676–705, https://doi.org/10.1175/1520-0442(1996)009<0676:ARLSPF>2.0.CO;2, 1996.

Sinclair, T. R. and Horie, T.: Leaf Nitrogen, Photosynthesis, and Crop Radiation Use Efficiency: A Review, Crop Sci, 29,
750   90–98, https://doi.org/10.2135/cropsci1989.0011183X002900010023x, 1989.

Takata, K., Emori, S., and Watanabe, T.: Development of the minimal advanced treatments of surface interaction and runoff, Glob Planet Change, 38, 209–222, https://doi.org/10.1016/S0921-8181(03)00030-4, 2003.

Tsvetsinskaya, E. A., Mearns, L. O., and Easterling, W. E.: Investigating the Effect of Seasonal Plant Growth and Development in Three-Dimensional Atmospheric Simulations. Part II: Atmospheric Response to Crop Growth and
755   Development, J Clim, 14, 711–729, https://doi.org/10.1175/1520-0442(2001)014<0711:ITEOSP>2.0.CO;2, 2001.

Tubiello, F. N. and Ewert, F.: Simulating the effects of elevated CO2 on crops: approaches and applications for climate change, European Journal of Agronomy, 18, 57–74, https://doi.org/10.1016/S1161-0301(02)00097-7, 2002.

Volkholz, J. and Müller, C.: ISIMIP3 soil input data (v1.0). ISIMIP Repository., https://doi.org/10.48364/ISIMIP.942125, 2020.

760 Volkholz, J. and Ostberg, S.: ISIMIP3a N-fertilizer input data (v1.2). ISIMIP Repository., https://doi.org/10.48364/ISIMIP.311496.2, 2022.

Vos, J., Van Der Putten, P. E. L., and Birch, C. J.: Effect of nitrogen supply on leaf appearance, leaf growth, leaf nitrogen economy and photosynthetic capacity in maize (Zea mays L.), Field Crops Res, 93, 64–73, https://doi.org/10.1016/J.FCR.2004.09.013, 2005.

765 Wu, X., Vuichard, N., Ciais, P., Viovy, N., De Noblet-Ducoudré, N., Wang, X., Magliulo, V., Wattenbach, M., Vitale, L., Di Tommasi, P., Moors, E. J., Jans, W., Elbers, J., Ceschia, E., Tallec, T., Bernhofer, C., Grünwald, T., Moureaux, C., Manise, T., Ligne, A., Cellier, P., Loubet, B., Larmanou, E., and Ripoche, D.: ORCHIDEE-CROP (v0), a new process-based agro-land surface model: Model description and evaluation over Europe, Geosci Model Dev, 9, 857–873, https://doi.org/10.5194/gmd-9-857-2016, 2016.

770 Yusara, A., Kato, T., Ainsworth, E. A., Battisti, R., Kumagai, E., Nakano, S., Wu, Y., Tsusumi-Morita, Y., Kobayashi, K., and Masutomi, Y.: Developing an eco-physiological process-based model of soybean growth and yield (MATCRO-Soy v.1): Model calibration and evaluation, EGUsphere[preprint], https://doi.org/10.5194/egusphere-2025-453, 2025.